LANGLEY RESEARCH CENTER
3 1176 00500 0816

DEC 22 1944

ACR No. L4I29

NATIONAL ADVISORY COMMITTEE FOR AERONAUTICS

WARTIME REPORT

ORIGINALLY ISSUED

September 1944 as
Advance Confidential Report L4I29

CHARTS FOR DETERMINING PROPELLER EFFICIENCY

By John L. Crigler and Herbert W. Talkin

Langley Memorial Aeronautical Laboratory
Langley Field, Va.

NACA

NACA LIBRARY

WASHINGTON

NACA WARTIME REPORTS are reprints of papers originally issued to provide rapid distribution of advance research results to an authorized group requiring them for the war effort. They were previously held under a security status but are now unclassified. Some of these reports were not technically edited. All have been reproduced without change in order to expedite general distribution.

NACA ACR No. L4I29

NATIONAL ADVISORY COMMITTEE FOR AERONAUTICS

ADVANCE CONFIDENTIAL REPORT

CHARTS FOR DETERMINING PROPELLER EFFICIENCY

By John L. Crigler and Herbert W. Talkin

SUMMARY

A short method of estimating propeller efficiency for a given operating condition is described. The efficiency is determined for any design condition by evaluating separately from charts the induced losses and the profile-drag losses. The estimated efficiency is compared with experimental results for a wide range of operating conditions and found to be in agreement near peak efficiency.

The present analysis covers single-rotating propellers of two, three, four, six, and eight blades and includes charts showing the rotational-energy loss for the given operating condition in order to assist in estimating the gain in efficiency for dual-rotating propellers. The change in efficiency to be expected from body interference is discussed. Two examples illustrating the use of the method are given in an appendix.

INTRODUCTION

In reference 1, analytically determined propeller performance is compared with experimental results for propellers having four, six, and eight blades of conventional design. The calculated results are in agreement with the experimental results over the complete range of blade angle investigated (25° to 65° at 0.75 radius). The calculations were made by a strip-theory analysis by which the thrust and torque contributions for several elements along the radius are graphically integrated for each operating condition. The time required to analyze a single operating condition by the strip-theory method is negligible compared with the time required to obtain experimental data for the same condition. The time required to analyze the

complete range of operation is considerable, however, and a shorter method is desirable.

A method of estimating the propeller performance supported by the results of reference 1 is presented herein. By this method, a large reduction in the time and effort required for propeller analysis is effected as compared with the strip-theory method. The results obtained are in agreement with those from experiment. The basic propeller parameters are interrelated in charts that aid in the selection of a propeller for a given design condition. The charts are useful in analyzing data for any propeller and aid in the determination of excessive losses.

The induced power losses for a conventional round-shank propeller are compared with the losses for the optimum load distribution. The induced losses are divided into axial- and rotational-energy losses so that the maximum gains possible by the use of dual-rotating propellers instead of optimum single-rotating propellers can be estimated. The effect of profile drag is treated separately. Because drag losses are evaluated separately, increased losses due to compressibility can be estimated directly when airfoil data at high Mach numbers become available.

Detailed applications of the method are illustrated by examples in the appendix.

SYMBOLS

a	axial-velocity interference factor
a'	rotational-velocity interference factor
B	number of propeller blades
b	chord of propeller blade element
C_D	section drag coefficient (D_o/qS)
C_L	section lift coefficient (L/qS)
C_P	power coefficient $(P/\rho n^3 D^5)$

[redacted]

C_Q	torque coefficient $(Q/\rho n^2 D^5)$
C_T	thrust coefficient $(T/\rho n^2 D^4)$
D	propeller diameter
D_o	drag of propeller blade element for infinite aspect ratio
E_a	axial energy per unit time in slipstream
E_r	rotational energy per unit time in slipstream
F	Goldstein correction factor for finite number of blades
J	advance-diameter ratio (V/nD)
L	lift of blade section
n	propeller rotational speed, revolutions per second
P	input power to propeller
P_c	power disk-loading coefficient (P/qSV)
Q	torque of propeller
q	dynamic pressure of air stream
R	tip radius
r	radius to any blade element
S	disk area of propeller
T	thrust of propeller
u_o	axial velocity in plane of propeller (propeller removed)
V	axial velocity of propeller
x	radial location of blade element (r/R)
dC_Q/dx	element torque coefficient $\left(\frac{dQ/dx}{\rho n^2 D^5}\right)$

[redacted]

dC_T/dx element thrust coefficient $\left(\frac{dT/dx}{\rho n^2 D^4}\right)$.

α_o angle of attack of blade element for infinite aspect ratio

β propeller blade angle at 0.75 radius

η propeller or element efficiency

ρ mass density of air

σ propeller element solidity ($Bb/2\pi r$)

σC_L propeller element load coefficient

ϕ angle of resultant velocity to plane of rotation $(\beta - \alpha_o)$

Subscripts:

0.7R at 0.7 radius

D due to drag

i for zero drag

FORMULAS

The derivation of the formulas for element thrust and torque calculations is given in reference 2, from which the element thrust coefficient is

$$\frac{dC_T}{dx} = \frac{BJ^2}{2} \frac{b}{R} \frac{(1 + a)^2}{\sin^2 \phi} (C_L \cos \phi - C_D \sin \phi) \qquad (1)$$

and the element torque coefficient is

$$\frac{dC_Q}{dx} = \frac{BJ^2 x}{16} \frac{b}{R} \frac{(1 + a)^2}{\sin^2 \phi} (C_L \sin \phi + C_D \cos \phi) \qquad (2)$$

[redacted]

The expression for the axial-velocity interference factor a is

$$\frac{a}{1 + a} = \frac{\sigma C_L \cot \phi}{4F \sin \phi} \tag{3}$$

(This equation neglects tip drag terms) See Ref. 5 p. 4.c

The values of the correction factor F as used in the present report are given in figure 1. The values of F for two-, three-, and four-blade propellers are taken from reference 3. The values of F for six- and eight-blade propellers were extrapolated from these data by the method developed in reference 3.

For calculations showing the effect of drag on propeller performance, the following formulas were obtained from equations (1) to (3) for $C_L = 0$:

$$\frac{dC_T}{dx} = -\sigma C_D \frac{\pi x}{4} J \sqrt{J^2 + (\pi x)^2}$$

$$= -\sigma C_D \frac{\pi x}{4} \frac{J^2}{\sin \phi} \tag{4}$$

$$\frac{dC_Q}{dx} = \sigma C_D \frac{\pi^2 x^3}{8} \sqrt{J^2 + (\pi x)^2}$$

$$= \sigma C_D \frac{\pi^2 x^3}{8} \frac{J}{\sin \phi} \tag{5}$$

Equations (4) and (5) are derived for zero loading without inflow and consequently are not exact for a finite loading. The formulas show, however, that the error in estimating the loss due to drag is negligible for light loadings which occur near peak propeller efficiency.

[redacted]

The formulas for the rotational-energy and axial-energy losses from reference 4 are

$$\frac{E_r}{P} = \frac{1}{C_Q} \int_0^{1.0} a' \frac{dC_Q}{dx} \, dx \tag{6}$$

$$\frac{E_a}{P} = \frac{J}{C_P} \int_0^{1.0} a \frac{dC_T}{dx} \, dx \tag{7}$$

where

$$a' = \frac{dC_Q}{dx} \frac{2}{\pi^2 J x^3 (1 + a) F}$$

and

$$a = \frac{-1 + \sqrt{1 + 4 \frac{dC_T/dx}{\pi x J^2 F}}}{2}$$

These formulas from reference 4 have been modified herein by inclusion of the correction factor F.

METHOD

Charts for Induced Losses

The basic propeller performance charts are presented in figure 2 for two-, three-, four-, six-, and eight-blade propellers. The ordinates represent values of the efficiency for propellers operating without drag and the abscissas represent values of $\frac{1}{\sqrt{P_{c_i}}} = D \sqrt{\frac{\pi \rho V^3}{8P}}$. Against these scales, curves of constant element load coefficient

[redacted]

$(\sigma C_L)_{0.7R}$ are crossed by long-dash lines of constant V/nD and short-dash lines of constant power coefficient C_{P_1}. The C_{P_1}-curves show the variation of $(\sigma C_L)_{0.7R}$ with V/nD for constant C_{P_1} and are included for convenience of computation for constant-speed propellers. The curves were obtained from calculated optimum torque and thrust distributions graphically integrated from the tip of the blade to $x = 0.2$. These performance charts are the same as the propeller selection charts in reference 5 except that the drag losses are not included.

In the present report, the value of the solidity at 0.7R, $\sigma_{0.7R}$, is taken as a convenient measure of the propeller solidity. The value of $(\sigma C_L)_{0.7R}$ is correspondingly taken as a measure of the power absorbed. The activity factor has frequently been taken as an index of the power-absorbing qualities of a propeller. For the Hamilton Standard 3155-6 propeller reported in reference 6 (for which comparisons are made in the present paper), the activity factor is 90 (per blade) and $\sigma_{0.7R}$ is 0.0345B; that is, for propellers of this design, the activity factor is $2600\frac{\sigma_{0.7R}}{B}$. This number is approximately the same for all conventional propellers. If the exact relationship is desired, however, the activity factor A.F. may be obtained from

$$\text{A.F.} = \frac{100000}{16} \int_{x=0.2}^{x=1.0} \frac{b}{D} x^3 \, dx$$

Breakdown of Propeller Power Losses

In the calculation of propeller efficiency, it has been customary to compute the thrust and torque at a given value of V/nD for a fixed blade-angle setting. The analytical determination of propeller performance may be considerably simplified in many cases, however, by evaluating the several sources of power loss rather than by attempting the direct computation of thrust and torque. In the present paper, the efficiency is

[redacted]

determined by deducting the sum of the power losses from unity. The total power losses are divided into induced losses and profile-drag losses; the induced losses are subdivided into axial- and rotational-energy losses for use in evaluating the efficiency of dual-rotating propellers. The blade drag has no appreciable effect on the induced losses for normal propellers but must be considered in obtaining the total power losses. This method of analysis has the advantage that compressibility corrections can be included when the airfoil section characteristics at the operating Mach number become known.

Rotational-energy losses.- The losses of efficiency due to rotational velocity are shown in figure 3 for three-, four-, six-, and eight-blade propellers. The rotational-energy loss for a given operating condition (constant P_c and V/nD) is seen to increase as the number of blades decreases. This increase in power loss arises from the increase in the tip loss as the number of blades decreases.

Calculations for a large number of load distributions show that overloading the inner radii is of secondary significance at values of operating $V/nD < 2.5$. As an illustrative case, the calculated rotational energy for the four-blade Hamilton Standard 3155-6 propeller of reference 6, which has round blade shanks, is compared in figure 4 with that for a four-blade propeller computed from the charts of figure 3. The rotational energy for the Hamilton Standard 3155-6 propeller was computed for several blade angles up to 65° at 0.75R and the value of V/nD for peak propeller efficiency. The values of E_r/P for the optimum propeller were taken from figure 3(b) at the same values of V/nD and P_c as for the Hamilton Standard 3155-6 propeller. Figure 4 shows that no appreciable difference in rotational energy exists between the two load distributions at $V/nD < 2.5$ and that the losses differ by only 1.5 percent of the total power at $V/nD = 4.5$, which corresponds to a blade-angle setting of 65° at 0.75R. The rotational-energy losses given in figure 3 are therefore close approximations to the expected losses for conventional round-shank propellers over the usual present-day operating range. Similar results are found even when airfoil sections are used over the inner radii when $V/nD < 2.5$. It cannot be emphasized too strongly, however, that if cuffs are used to cover the round

[redacted]

shanks, the loss may become serious at high values of V/nD unless the cuffs are set at an angle of attack between 0° and the optimum to give low loading over these sections. This dependence of the rotational energy in the slipstream on the loading over the inner radii is apparent from equation (6), which shows how the effect of overloading the inner radii increases in importance as the operating V/nD increases.

Axial-energy losses.- The axial-energy loss for any operating condition may be obtained from the relationship

$$\frac{E_a}{P} = 1 - \eta_i - \frac{E_r}{P}$$

where the induced efficiency η_i is obtained from figure 2 and E_r/P is obtained from figure 3. The axial-energy loss shows but little variation among propellers in present-day usage operating near peak efficiency. As an illustration, the axial-energy losses for a four-blade propeller obtained from the charts of figures 2 and 3 are compared in figure 5 with the calculated values for the four-blade Hamilton Standard 3155-6 propeller operating at peak propeller efficiency and for the ideal propeller (actuator disk). The values of P_c at V/nD for peak efficiency for the Hamilton Standard 3155-6 propeller were taken from reference 6. The axial-energy losses for the optimum propeller load distribution and for the ideal propeller were determined at the same values of V/nD and P_c as for the Hamilton Standard 3155-6 propeller. The axial-energy losses for the optimum distribution of loading (figs. 2 and 3) and for the loading obtained with the Hamilton Standard 3155-6 propeller are nearly equal and are about 1 percent higher than for the ideal propeller over the range investigated. A part of this increase in axial-energy loss is due to the finite number of blades and therefore becomes less as the number of blades increases. A small part of the difference occurs because the load distribution differs from that of an actuator disk. The axial-energy loss for optimum distribution, obtained with the aid of figures 2 and 3, is therefore sufficiently accurate for application to conventional propellers.

[redacted]

Blade-drag losses.- The effect of blade drag on the characteristics of lightly loaded propellers (near peak efficiency) can be estimated from equations (4) and (5). These equations were obtained by eliminating the axial inflow and putting $C_L = 0$ in equations (1) and (2). The equations are not exact but, near peak efficiency for modern high-speed propellers, the omission of the inflow factor a causes a negligible change in the calculated propeller efficiency. Equations (4) and (5) show that, for a given radius and value of V/nD, the element thrust and torque coefficients due to drag are directly proportional to the drag coefficient.

The profile-drag coefficients for infinite aspect ratio for several sections along the Hamilton Standard 3155-6 blade are shown against lift coefficient in figure 6. These data were taken from reference 7. The profile-drag coefficients change with lift coefficient but, since the change is very small for a wide range of lift coefficient, average values were used in the calculations for operation near peak efficiency. The profile-drag coefficient increases rapidly near the stalling angle of the section and the average values are accordingly not representative for such conditions.

Figures 7 and 8 show the effect of drag on the thrust and torque coefficients, respectively, for several values of V/nD. The values of the section profile-drag coefficient shown in figures 7 and 8 were used in the calculations for the Hamilton Standard 3155-6 propeller. Curves of the differential-thrust and differential-torque corrections due to drag, for the drag coefficients shown, are plotted against the radial location x, and the integrated corrections are also included in figures 7 and 8. These integrated values apply for one blade and the correction is directly proportional to the number of blades and to the blade chord. The element thrust coefficient and the element torque coefficient due to drag at a given value of V/nD are directly proportional to C_D, and a change in C_D at any radius is represented by a proportional change in the ordinate of the differential-thrust and differential-torque curves. For this reason, the method of analysis is adaptable to any blade section for which the airfoil characteristics are available. The suggestion is also made that the loss in efficiency due to drag at high speeds at which the blade section drag becomes large

[redacted]

can be predicted when the drag coefficients at high Mach numbers become available. The calculations show that the drag correction to the thrust is chiefly due to the high drag of the inner sections (see fig. 7) and that a change in the drag coefficient of the principal working part of the blade due to a change in the lift coefficient near peak efficiency (see fig. 6) results in a negligible change in the correction to the thrust coefficient.

The effect of drag on the efficiency envelope and on the integrated power coefficient for operation at peak efficiency in unobstructed air flow is shown in figure 9. The values of η_i and the corresponding C_{P_i} without drag were taken from figure 2 for four-blade propellers at $(\sigma C_L)_{0.7R} = 0.07$. For optimum distribution of loading along the radius for the solidity of the four-blade Hamilton Standard 3155-6 propeller, this value of $(\sigma C_L)_{0.7R}$ corresponds to $C_{L_{0.7R}} = 0.51$. The solid lines in figure 9 give the maximum efficiency and the corresponding power coefficients against V/nD for optimum distribution for a four-blade frictionless propeller at $(\sigma C_L)_{0.7R} = 0.07$. The short-dash lines show η and C_P as modified by blade drag integrated from 0.20R to the tip. The curve for η for blade drag integrated from 0.45R to the tip is shown by the long-dash line. The C_P-curve is not shown for the latter case but falls between the other C_P-curves.

The introduction of blade drag of the magnitude shown in figures 7 and 8 has little effect on the total power absorbed during operation near peak efficiency, regardless of V/nD; the effect of the drag on the integrated thrust and hence on the efficiency, however, is important and increases rapidly with V/nD. For example, the loss in efficiency for the entire blade varies from 5.5 percent at $\frac{V}{nD} = 1.0$ to 23.0 percent at $\frac{V}{nD} = 6.0$. On the other hand, the loss in efficiency due to the drag of the principal working sections - that is, from 0.45R to the tip - is relatively unimportant. The loss in efficiency for this portion of the blade (see long-dash line, fig. 9) is thus seen to vary from 2.5 percent at $\frac{V}{nD} = 1.0$ to 4.0 percent at $\frac{V}{nD} = 6.0$; these losses

[redacted]

represent the upper limits for increases in efficiency that may be achieved by reducing the profile drag for the working sections of the blade operating at $C_L = 0.51$ with optimum load distribution. The thick inner sections of conventional round-shank propellers, which are used for structural reasons, are therefore the chief source of blade-drag loss, especially at high values of V/nD. This loss in efficiency due to drag may be greatly reduced by covering the inner portion of the shank with a spinner and the outer portion with cuffs, if the cuff angle is properly set. It is emphasized that cuffs may result in a loss in efficiency instead of a gain unless set at the proper angle of attack. Overloading of the inner radii results in a large increase in the power in rotational energy for single-rotating propellers, and the blade-drag loss also becomes large for blade sections operating near the stall.

The losses due to the thick inner sections are also reduced when the propeller is operating in front of a blunt body, such as an NACA cowling, because of the low velocity over these sections. Calculations of thrust and torque coefficients have therefore been made at the same values of V/nD and for the same distribution of the element drag coefficients as in figures 7 and 8 but with the inner portion of the blade assumed to be operating in a region of low-velocity air as in front of a conventional air-cooled installation. The velocity distribution in the plane of the propeller, as used in these calculations, is given in figure 10, for which the data are taken from reference 4. The region of low-velocity air depends on the ratio of the nacelle diameter to the propeller diameter, the conductance of the engine, and the distance of the propeller in front of the cowling. The ratio of the nacelle diameter to the propeller diameter in the setup in reference 4 was 0.417. The effect of operation in front of an open-nose cowling (velocity distribution of fig. 10) is shown in figures 11 and 12 for a four-blade propeller. Thrust and power coefficients due to the distribution of drag in figures 7 and 8 are shown for free-stream operation by short-dash lines in figure 11; the long-dash lines represent operation in front of the NACA cowling. The value of the power coefficient due to drag $(\Delta C_P)_D$ is seen to vary but little with V/nD whereas $(\Delta C_T)_D$ rises rapidly.

[redacted]

Equations (4) and (5) also show this effect. The effect on the efficiency of operating a propeller in the velocity distribution of figure 10 is shown in figure 12 and compared with the efficiency computed for operation in free stream. The increase in propeller efficiency resulting from the presence of the cowling varies from 1.0 percent at $\frac{V}{nD} = 1.0$ to 9.0 percent at $\frac{V}{nD} = 6.0$. In the calculations for the curves shown in figure 12, the only variation considered is the drag of the blade shanks. The low-velocity air causes an increase in lift over the outer sections of the shank and, accordingly, an increase in the rotational-energy loss, which may result in a somewhat smaller gain in propeller efficiency than indicated by figure 12. In order to determine exactly the magnitude of the change in propeller efficiency, element calculations for each velocity distribution are necessary inasmuch as a change in velocity distribution produces an effective change in pitch distribution.

COMPARISON WITH EXPERIMENT

The experimental efficiency envelopes for four-, six-, and eight-blade Hamilton Standard 3155-6 propellers are compared with the calculated results integrated to 0.20R in figure 13. The experimental results for the four- and six-blade propellers were taken from reference 6 and the results for the eight-blade propeller were taken from reference 8. The single-rotating propellers were made up of two hubs mounted in tandem. The spinner in the setup for all the experimental data covered the inner 0.189R of the front unit of one-half the blades and the inner 0.232R of the rear blades. The results are in agreement over the entire range investigated for each set of blades. The calculated efficiency is about 1 percent lower than the experimental efficiency at low values of V/nD and is higher than the experimental efficiency at very high values of V/nD; the calculated curve crosses the experimental curve at $V/nD \approx 3.5$. Part of the discrepancy is due to the use of the short method.

[redacted]

CONCLUSIONS

A short method of estimating propeller efficiency for a given operating condition has been developed by a theoretical analysis. The efficiency is determined by evaluating separately the induced losses and the profile-drag losses. A comparison of the estimated efficiencies with experimental results indicated the following conclusions:

1. The performance for operation at values of the advance-diameter ratio equal to or less than 2.5 may be accurately predicted.

2. The approximate performance of conventional round-shank propellers may be predicted to values of the advance-diameter ratio much higher than 2.5.

3. The upper limit of possible performance for other types of propeller (airfoil sections over the inner radii or the use of cuffs over the round shanks) is shown for values of the advance-diameter ratio up to 6.0.

4. The cause of excessive losses may be determined for any propeller design.

5. The maximum gain in efficiency to be realized with dual-rotating propellers over optimum single-rotating propellers is evaluated for a wide range of operating condition.

Langley Memorial Aeronautical Laboratory
National Advisory Committee for Aeronautics
Langley Field, Va.

[redacted]

APPENDIX

APPLICATION OF THE METHOD

The problem of determining the propeller efficiency for a given design condition by the methods of the present report may be resolved into two parts: (1) determination of the induced power losses and (2) determination of the profile-drag losses. The induced power losses for a given design condition are available from figure 2 as $1 - \eta_i$. The induced losses obtained from figure 2 at $V/nD < 2.5$ are very close approximations to those obtained with conventional propellers. This range of V/nD covers most current high-speed designs. The blade drag is handled separately and can therefore be used for high Mach numbers and high drags if the correct airfoil section characteristics are used for the corresponding Mach numbers. The profile-drag losses are obtained from figure 11, which shows the variation of the thrust and power coefficients due to drag for the values of the element drag coefficients shown in figures 7 and 8. These drag values are representative for the Hamilton Standard 3155-6 propeller operating near peak efficiency. The ordinates of the curves in figures 7 and 8 are directly proportional to the drag coefficients at each radius so that, if other drag values are used, new curves giving the thrust and power coefficients due to drag may be easily plotted. Since the total power losses are divided into induced power losses and profile-drag losses, the method aids in determining excessive losses for any design condition. Excessive losses may be due to the fact that the propeller is either too heavily loaded or too lightly loaded, to a poor load distribution along the blade, or to high blade drag due to compressibility. The use of the performance charts determines the lift coefficient at a representative station and thus the loading.

Two examples are given to illustrate the use of the charts in the determination of the propeller efficiency for a given design condition.

Example 1

In example 1, the propeller selected operates on a liquid-cooled installation in the tractor position and all the sections are assumed to operate at free-stream velocity. No compressibility corrections are applied.

[redacted]

The following design conditions are assumed:

Power, hp	2000
Altitude, ft	25,000
Velocity, mph	425
Rotational speed, rps	23
Propeller diameter, ft	12
Number of blades	Four
$\sigma_{0.7R} = \frac{Bb}{2\pi r}$	0.1380
Activity factor	90
V/nD	2.26
$C_P = \frac{P}{\rho n^3 D^5}$	0.342

The calculated values for operation in free air are

$(\Delta C_P)_D$ (fig. 11)	0.006
$C_{P_i} = C_P - (\Delta C_P)_D$	0.336
$1/\sqrt{P_{c_i}}$	3.67
$(\sigma C_L)_{0.7R}$ (fig. 2(c))	0.07
$C_{L_{0.7R}}$	0.51
η_i (fig. 2(c))	0.931
E_r/P (fig. 3(b))	0.039
$C_{T_i} = \frac{\eta_i C_{P_i}}{V/nD}$	0.1385
$(\Delta C_T)_D$ (fig. 11)	-0.0103
$C_T = C_{T_i} + (\Delta C_T)_D$	0.1282
$\eta = \frac{C_T}{C_P}\frac{V}{nD}$	0.848

In order to determine whether the propeller selected is loaded properly, the value of $C_{L_{0.7R}}$ is first determined in the selection chart in figure 2. Since the design conditions are given and $1/\sqrt{P_{c_i}}$ and V/nD have been predetermined, the value of $(\sigma C_L)_{0.7R}$ is read directly from the chart. The value of $C_{L_{0.7R}}$ required

[redacted]

is found to be 0.51 and indicates a satisfactory design condition. This lift coefficient has been found to be that absorbed near peak propeller efficiency for the Hamilton Standard 3155-6 propeller for operation at the given V/nD. The power loss due to rotational velocity E_r/P, which is equal to 0.039, is the maximum increase in efficiency to be expected from the use of dual-rotating propellers of the same diameter and solidity. The induced efficiency is 0.93 but the introduction of drag of the magnitude of that shown in figures 7 and 8 reduces the over-all propeller efficiency to 0.848. The use of $1/\sqrt{P_c}$ with drag included, instead of $1/\sqrt{P_{c_i}}$, results in negligible changes in η_i and $(\sigma C_L)_{0.7R}$.

Example 2

The only difference between example 2 and example 1 is that the propeller in example 2 is mounted in front of an open-nose cowling (air-cooled installation) with the inner sections of the propeller in retarded air flow.

The design conditions, which are the same as in example 1, are

Power, hp	2000
Altitude, ft	25,000
Velocity, mph	425
Rotational speed, rps	23
Propeller diameter, ft	12
Number of blades	Four
$\sigma_{0.7} = \frac{Bb}{2\pi r}$	0.1380
Activity factor	90
V/nD	2.26
$C_P = \frac{P}{\rho n^3 D^5}$	0.342

The calculated values for operation in front of NACA cowling are

$(\Delta C_P)_D$ (fig. 11)	0.006
$C_{P_i} = C_P - (\Delta C_P)_D$	0.336
$1/\sqrt{P_{c_i}}$	3.67

$(\sigma C_L)_{0.7R}$ (fig. 2(c))	0.07
$C_{L_{0.7R}}$	0.51
η_1 (fig. 2(c))	0.931
E_r/P (fig. 3(b))	0.039
$C_{T_1} = \frac{\eta_1 C_{P_1}}{V/nD}$	0.1385
$(\Delta C_T)_D$ (fig. 11)	-0.0065
$C_T = C_{T_1} - (\Delta C_T)_D$	0.1320
$\eta = \frac{C_T}{C_P}\frac{V}{nD}$	0.872

[redacted]

REFERENCES

1. Crigler, John L.: Comparison of Calculated and Experimental Propeller Characteristics for Four-, Six-, and Eight-Blade Single-Rotating Propellers. NACA ACR No. 4B04, 1944.

2. Glauert, H.: Airplane Propellers. Vol. IV of Aerodynamic Theory, div. L., W. F. Durand, ed., Julius Springer (Berlin), 1935, pp. 169-360.

3. Lock, C. N. H., and Yeatman, D.: Tables for Use in an Improved Method of Airscrew Strip Theory Calculation. R. & M. No. 1674, British A.R.C., 1935.

4. Stickle, George W., and Crigler, John L.: Propeller Analysis from Experimental Data. NACA Rep. No. 712, 1941.

5. Crigler, John L., and Talkin, Herbert W.: Propeller Selection from Aerodynamic Considerations. NACA ACR, July 1942.

6. Biermann, David, and Hartman, Edwin P.: Wind-Tunnel Tests of Four- and Six-Blade Single- and Dual-Rotating Tractor Propellers. NACA Rep. No. 747, 1942.

7. Pinkerton, Robert M., and Greenberg, Harry: Aerodynamic Characteristics of a Large Number of Airfoils Tested in the Variable-Density Wind Tunnel. NACA Rep. No. 628, 1938.

8. Biermann, David, and Gray, W. H.: Wind-Tunnel Tests of Eight-Blade Single- and Dual-Rotating Propellers in the Tractor Position. NACA ARR, Nov. 1941.

[redacted]

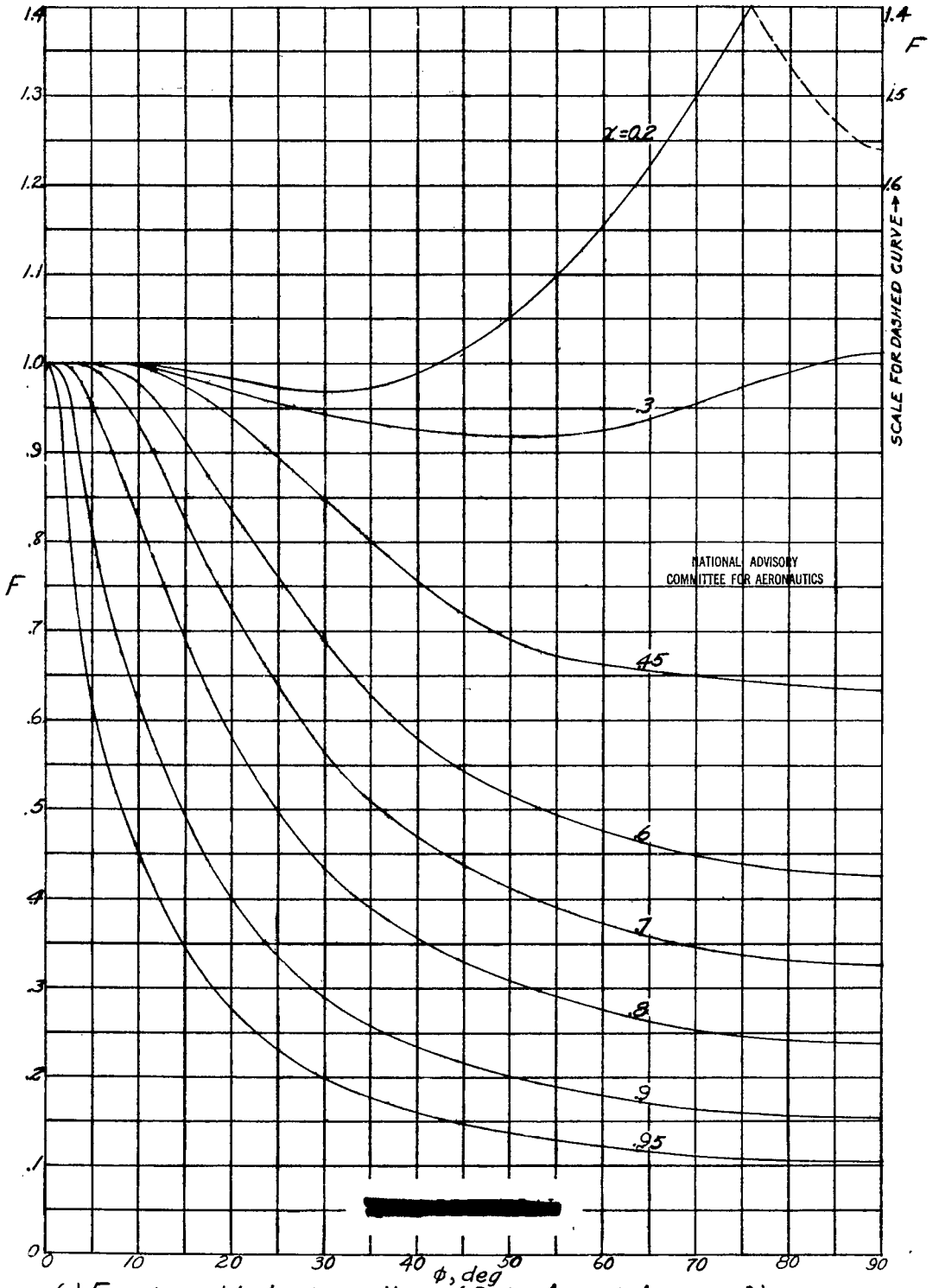

(a) For two-blade propellers. (Data from reference 3.)

Figure 1.- Curves of F against φ.

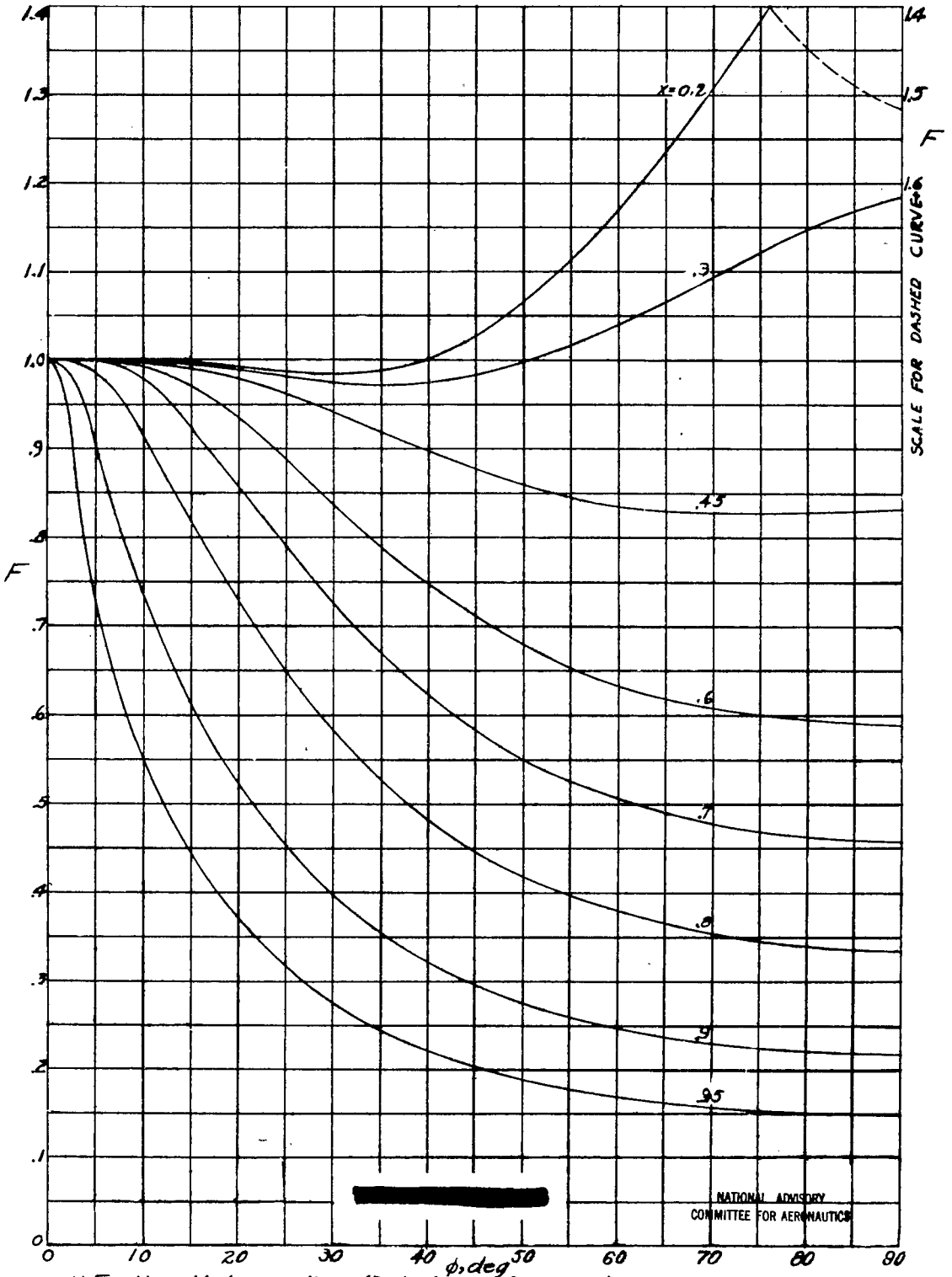

(b) For three-blade propellers. (Data from reference 3.)

Figure 1.— Continued.

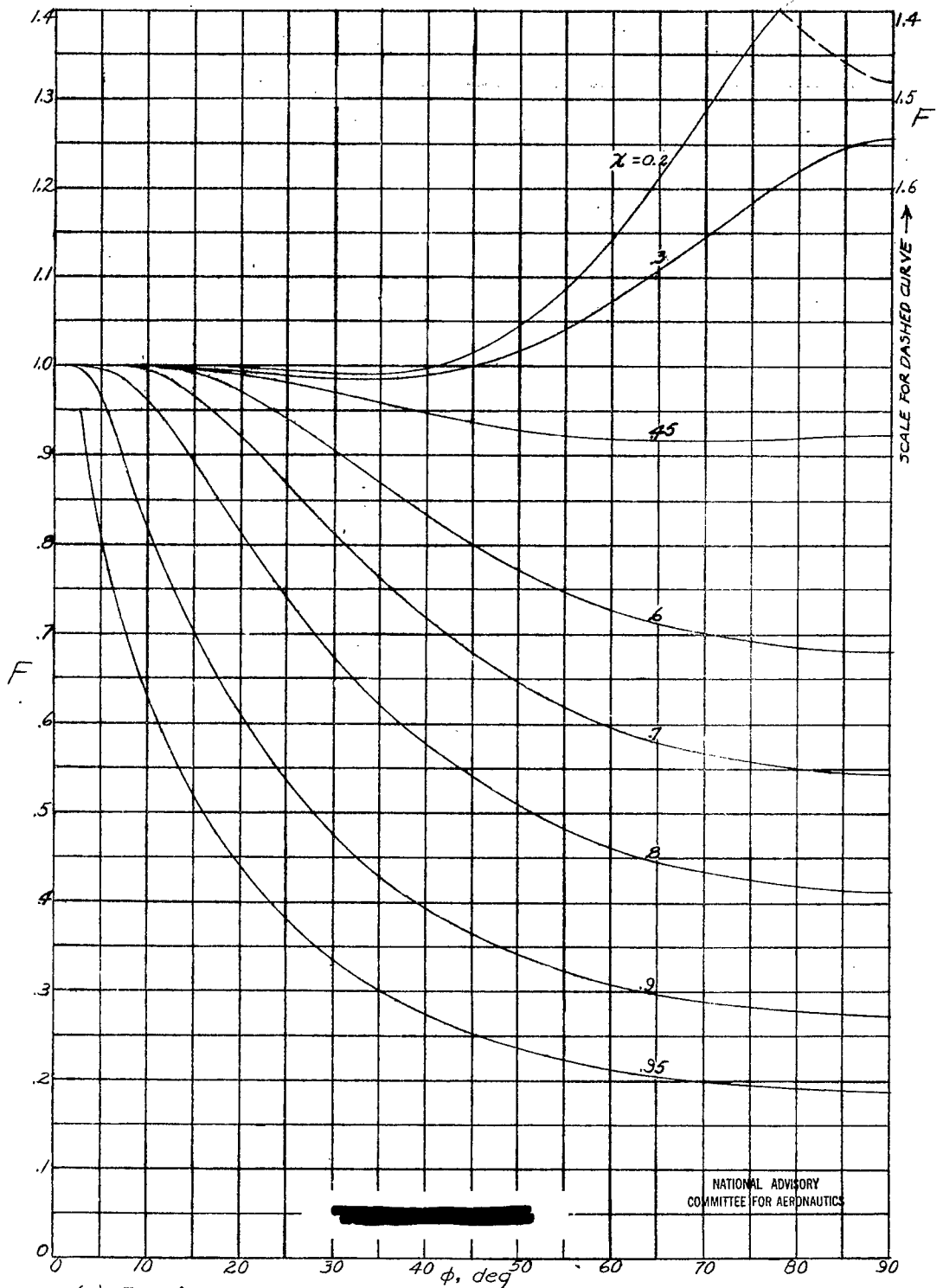

(c) For four-blade propellers. (Data from reference 3.)

Figure 1.- Continued.

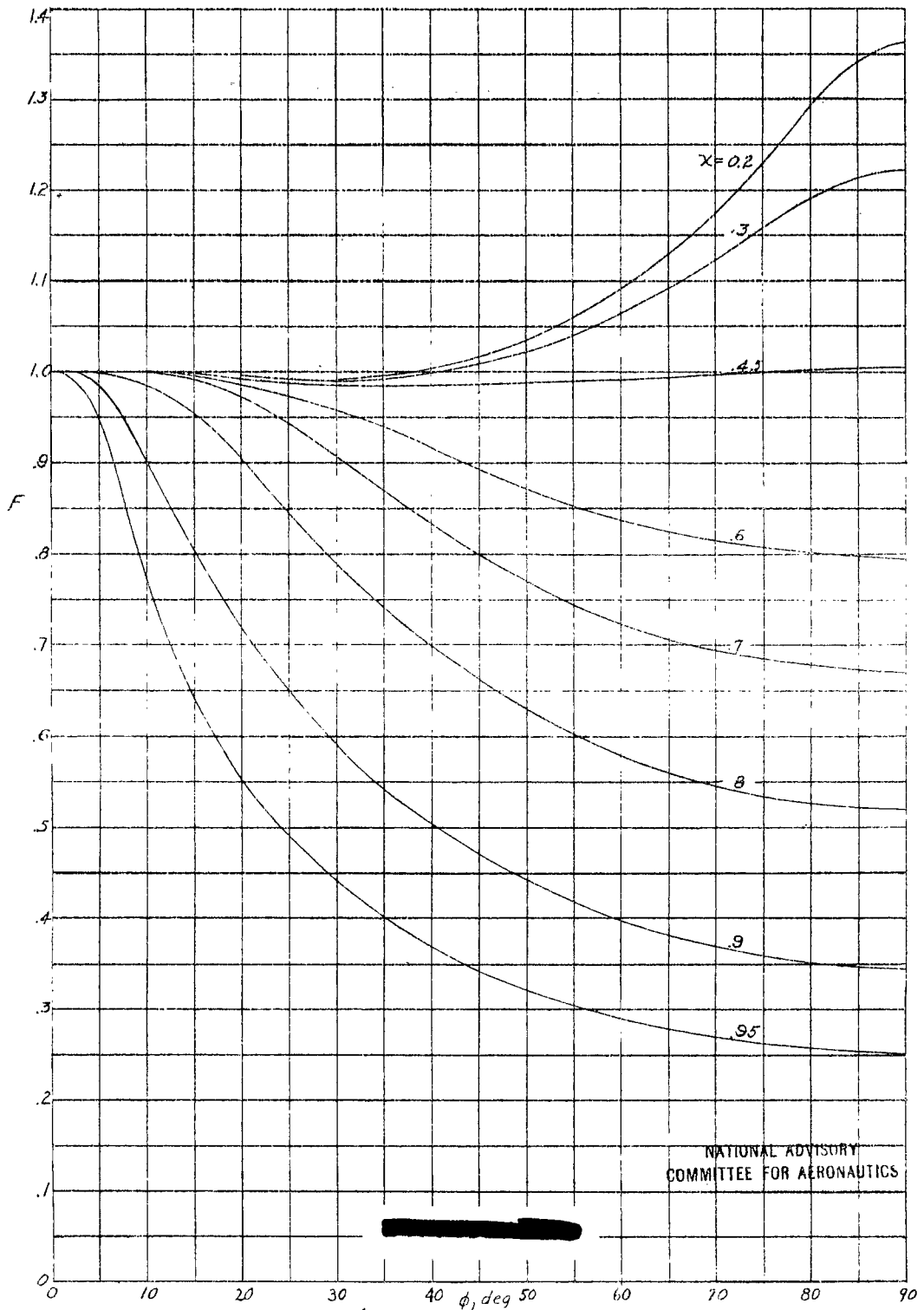

(d) For six-blade propellers. (Extrapolated from reference 3.)

Figure 1.- Continued.

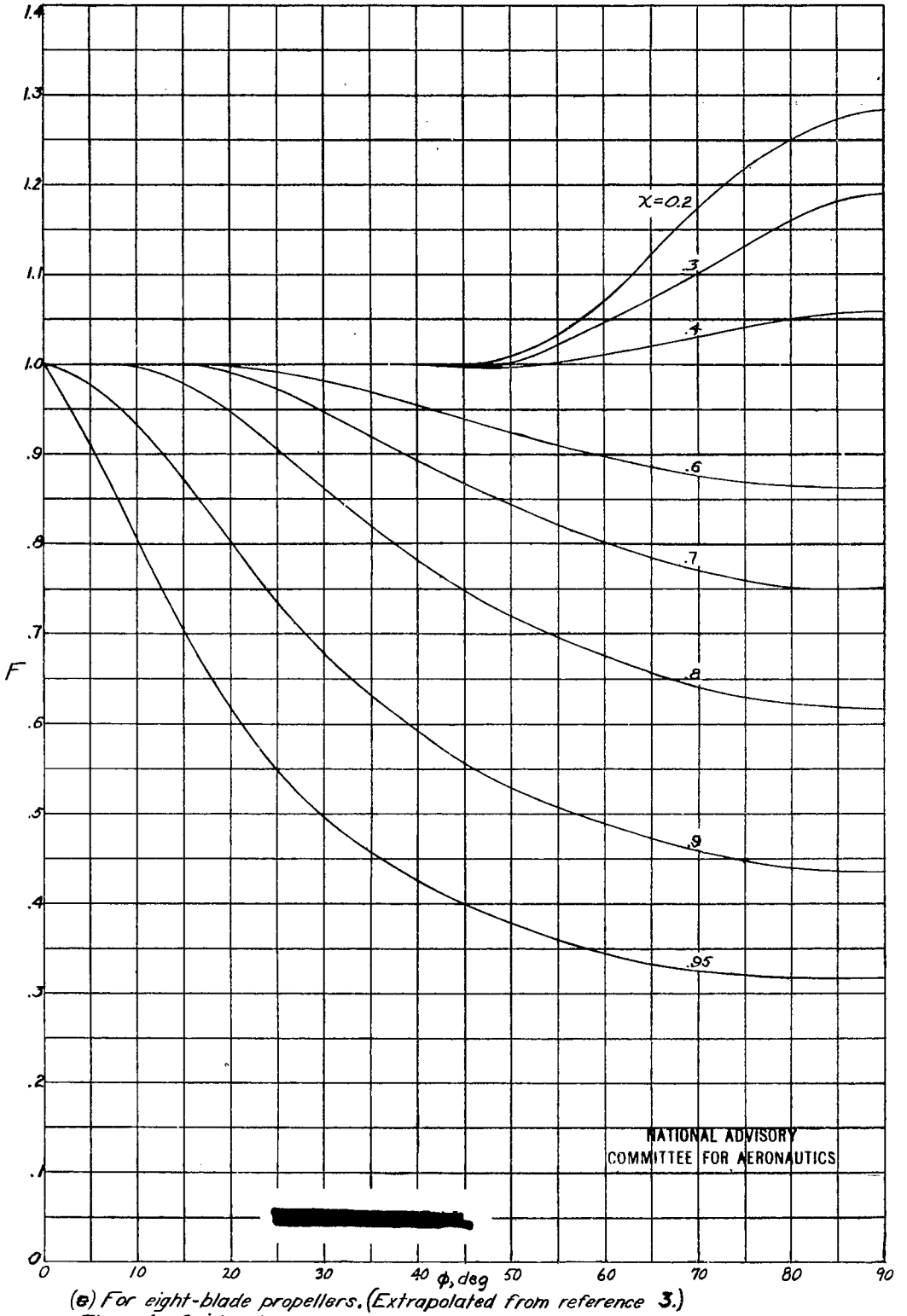

(e) For eight-blade propellers. (Extrapolated from reference 3.)

Figure 1. - Concluded.

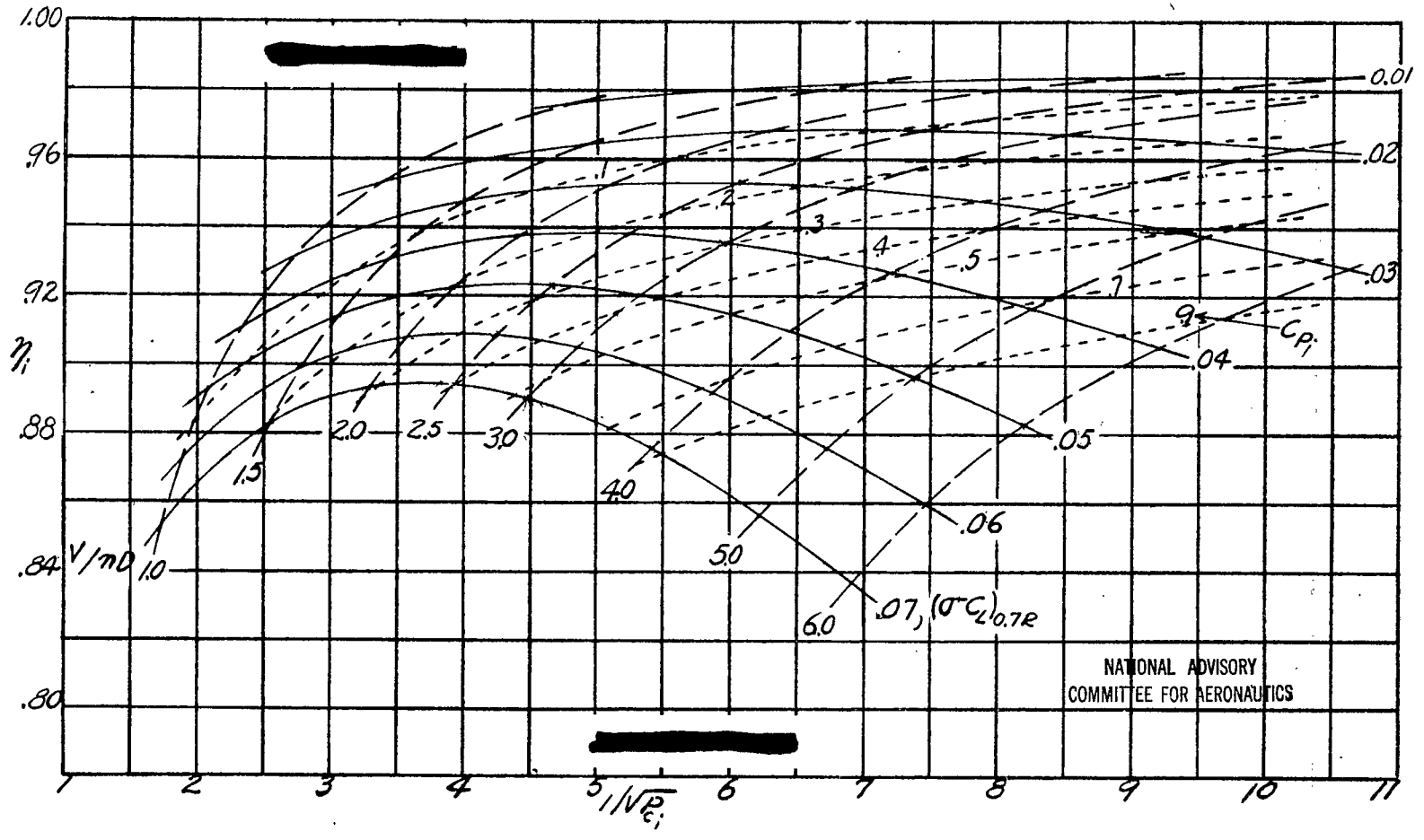

(a) Two-blade propellers.

Figure 2.- Propeller performance chart. Without drag.

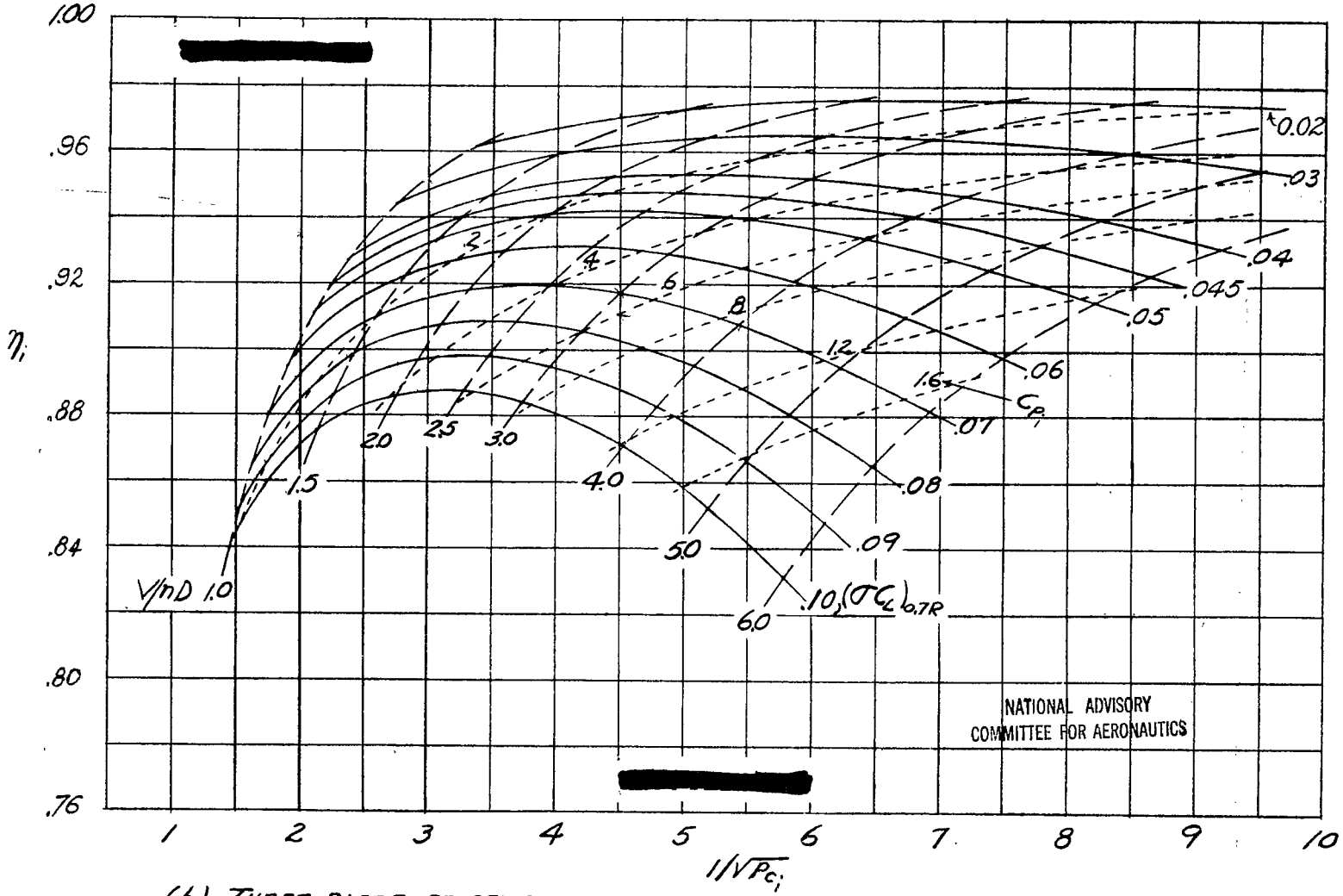

(b) THREE-BLADE PROPELLERS.

FIGURE 2.- CONTINUED.

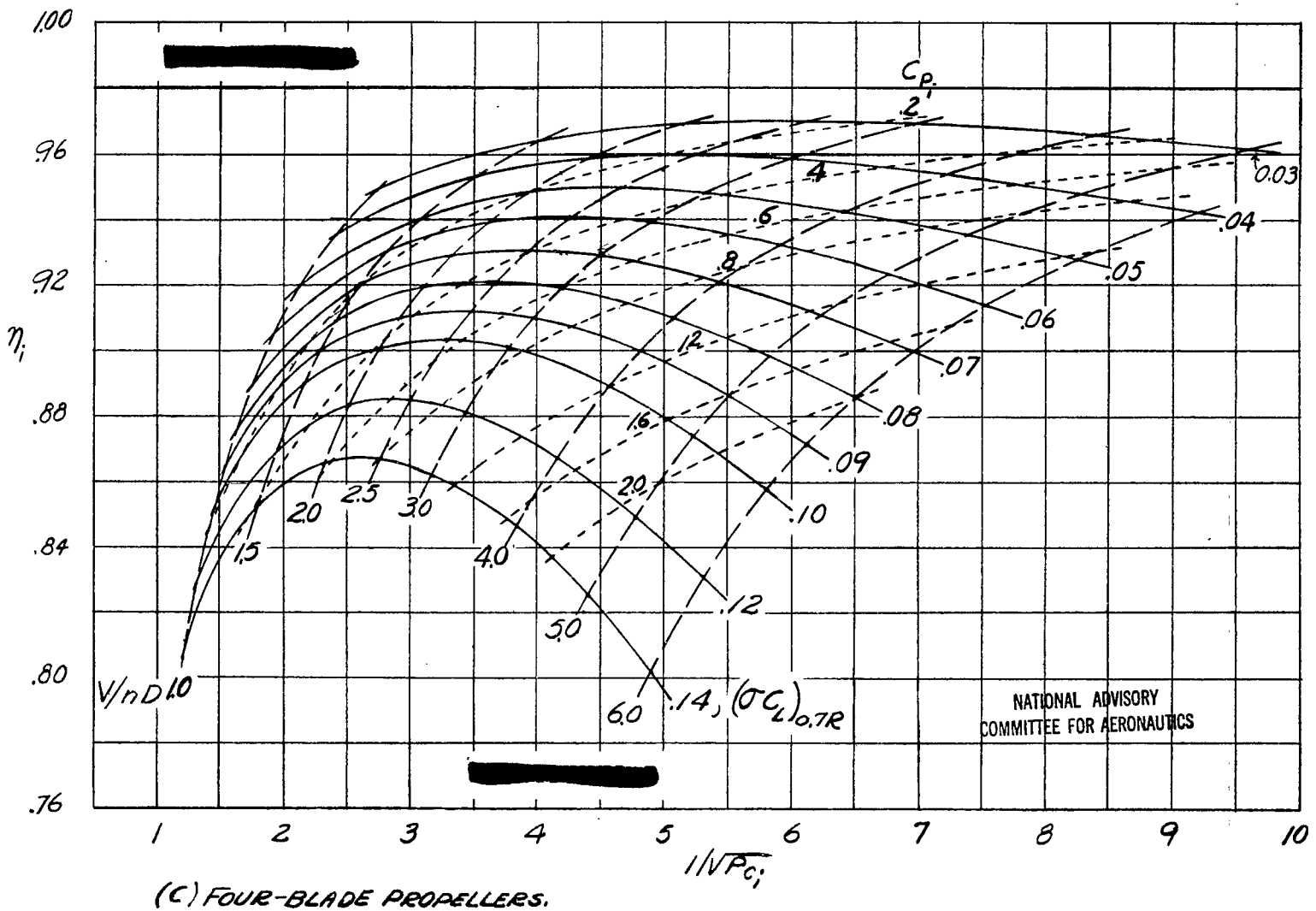

(C) FOUR-BLADE PROPELLERS.

FIGURE 2.- CONTINUED.

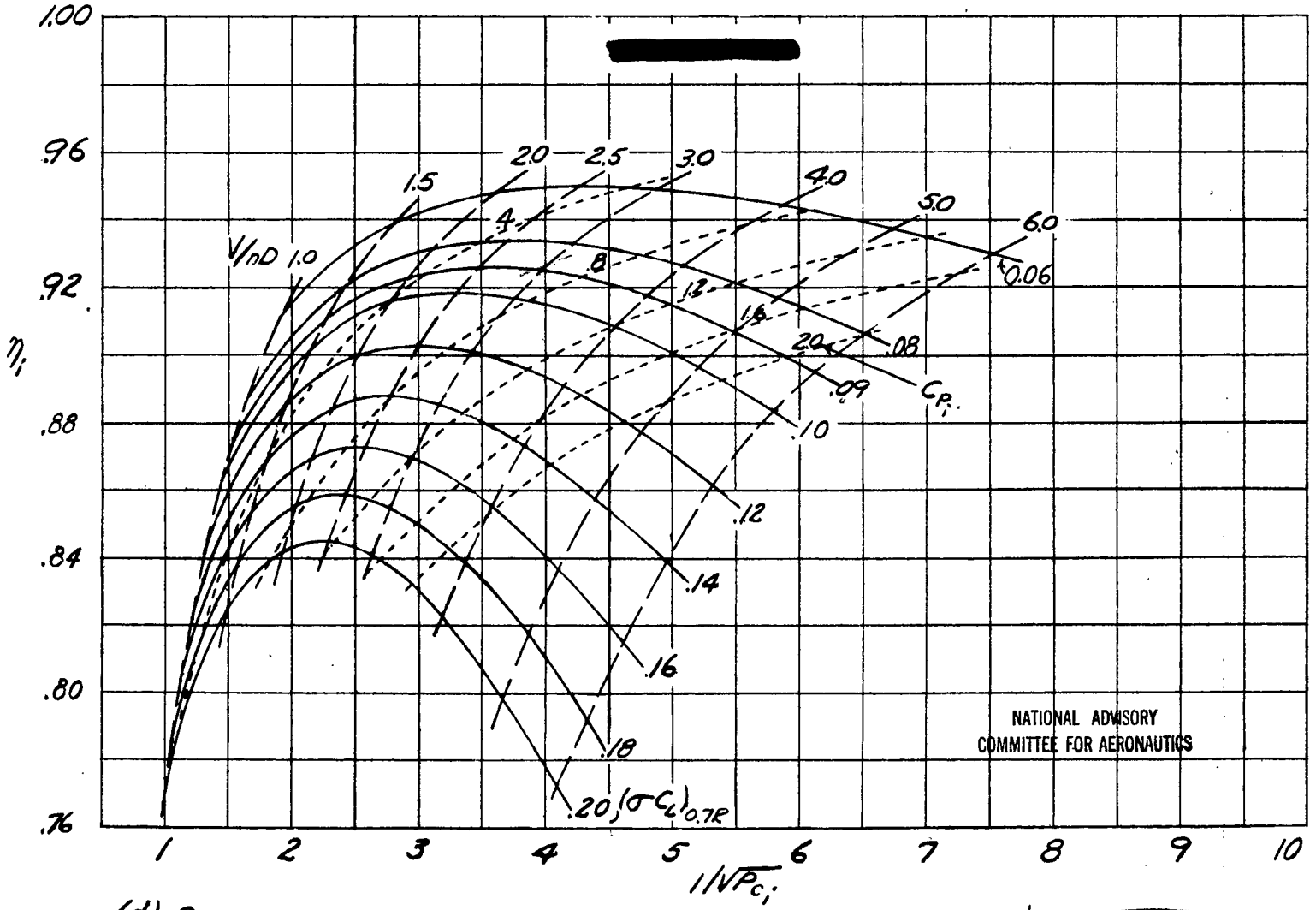

(d) SIX-BLADE PROPELLERS.

FIGURE 2.-CONTINUED.

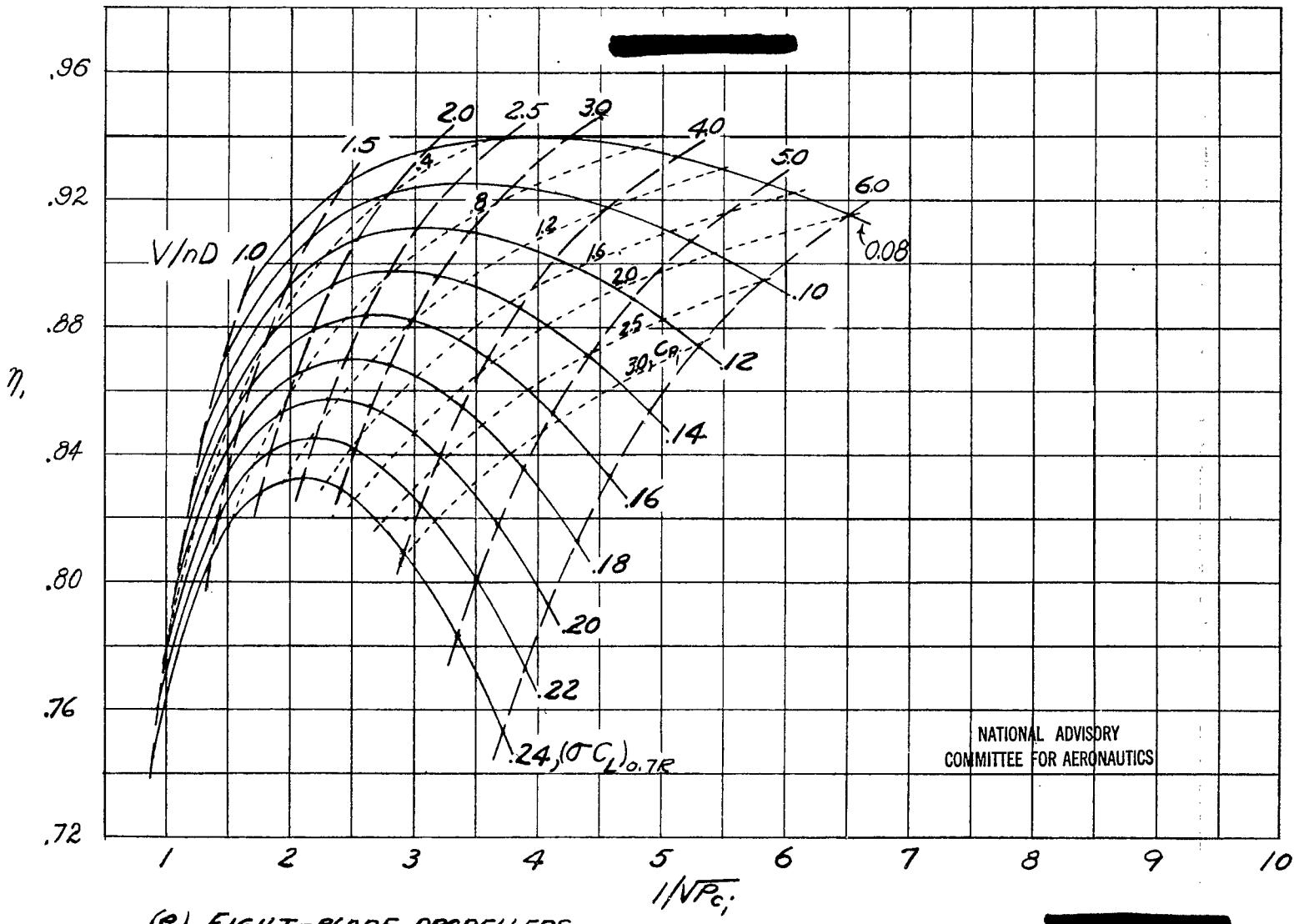

(e) EIGHT-BLADE PROPELLERS.

FIGURE 2.- CONCLUDED.

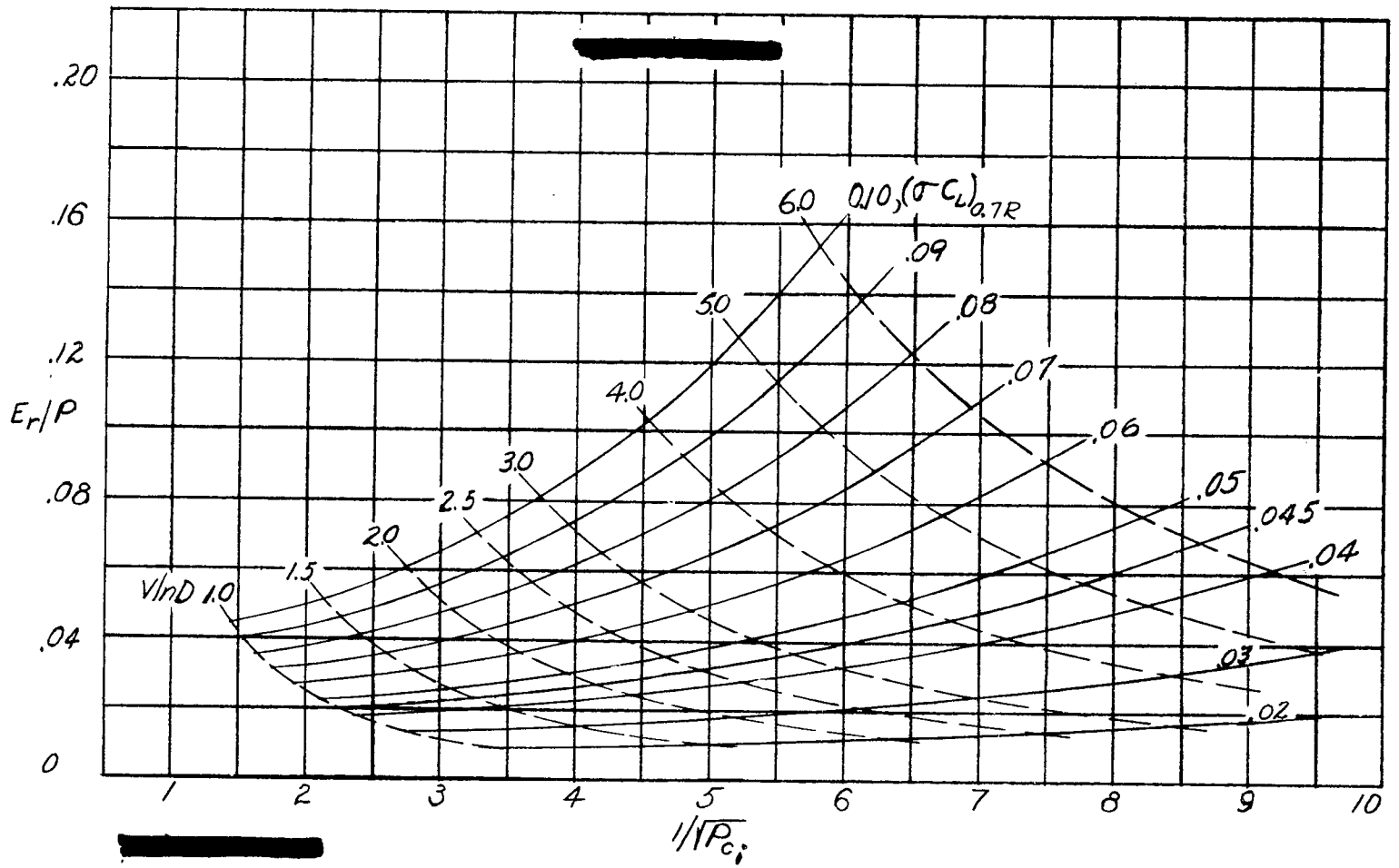

NATIONAL ADVISORY
COMMITTEE FOR AERONAUTICS

(a) THREE-BLADE PROPELLERS.

FIGURE 3.- LOSS OF EFFICIENCY DUE TO ROTATIONAL VELOCITY.

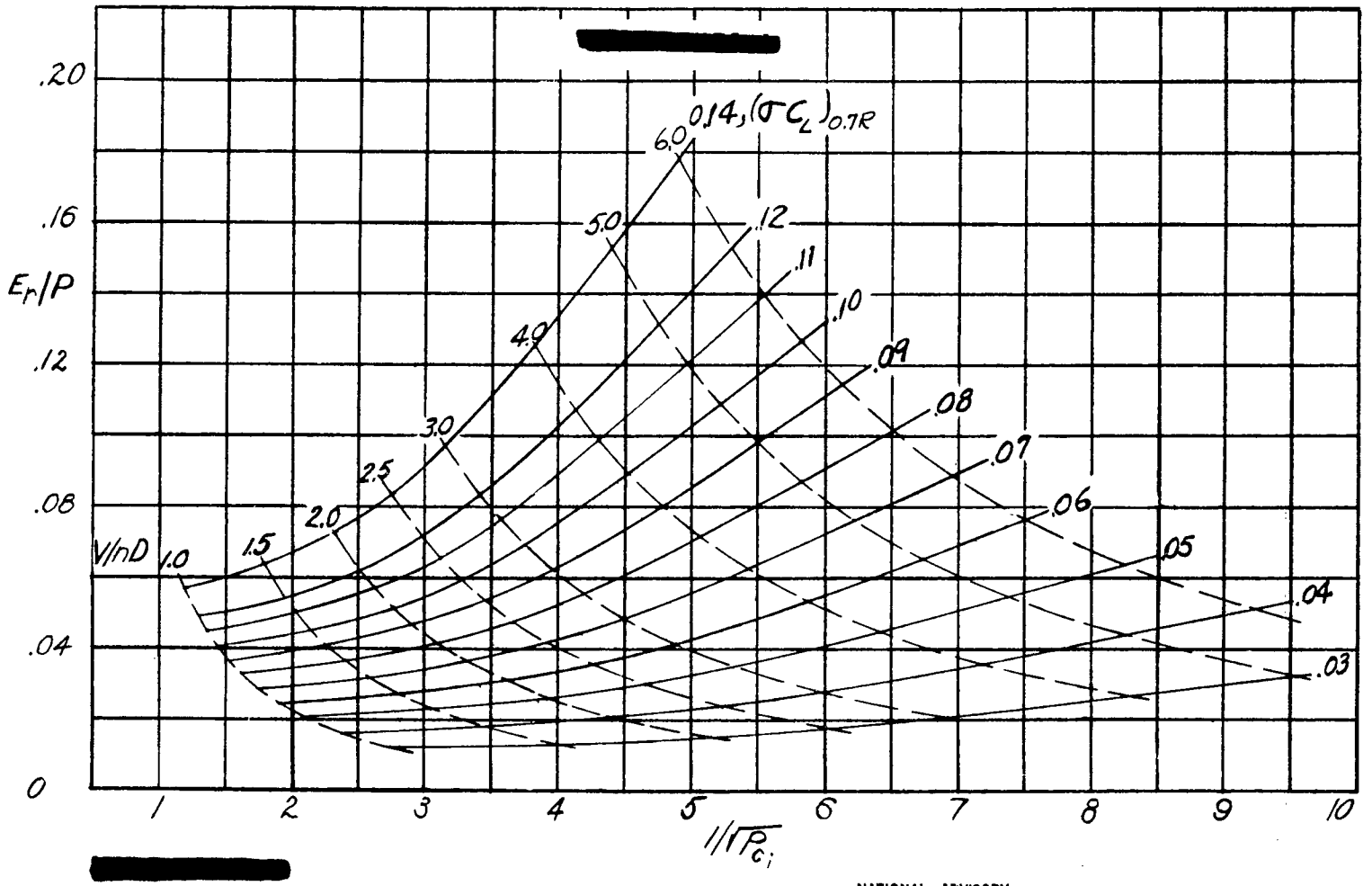

(b) FOUR-BLADE PROPELLERS.

FIGURE 3.- CONTINUED.

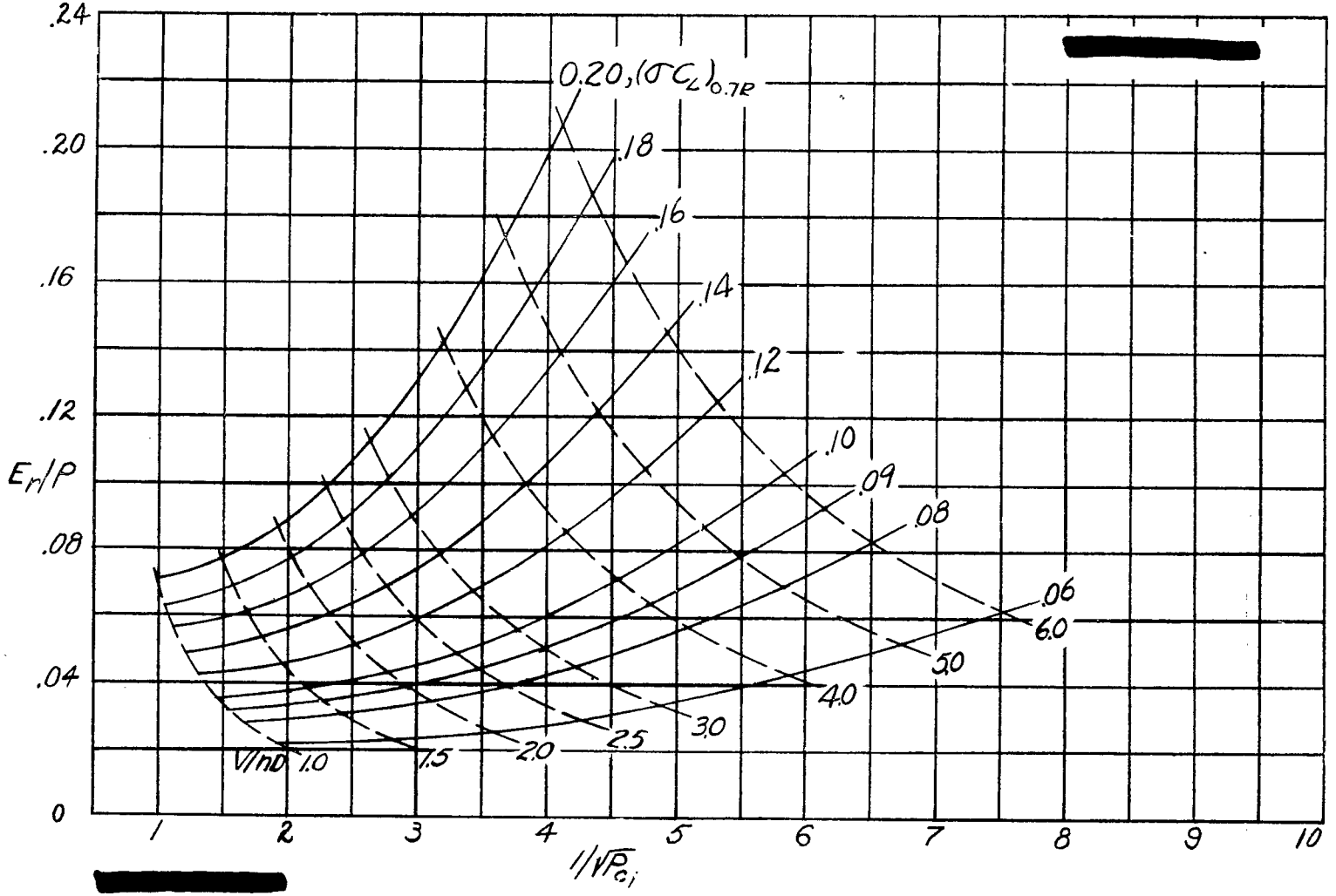

(C) SIX-BLADE PROPELLERS.

FIGURE 3.- CONTINUED.

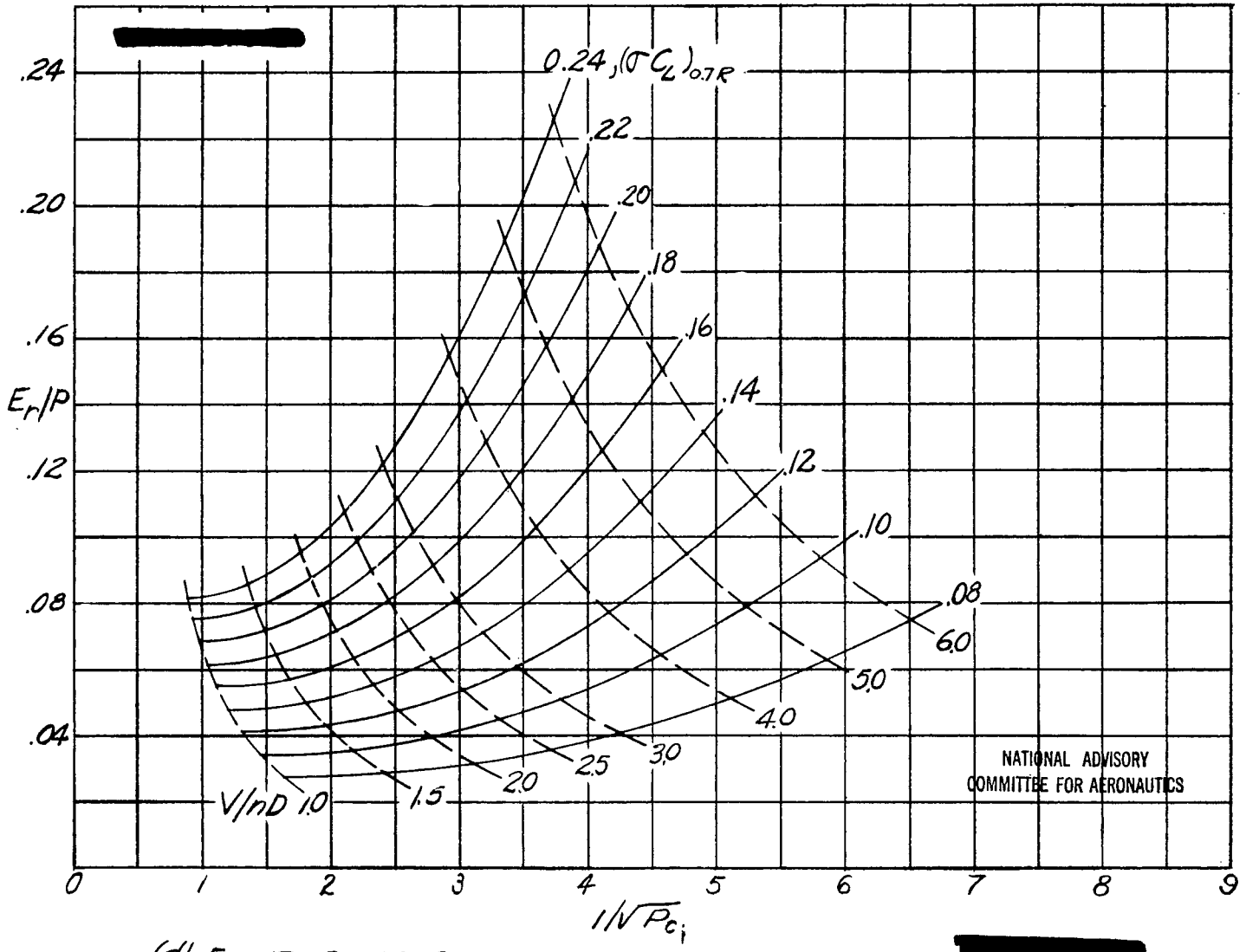

(d) EIGHT-BLADE PROPELLERS.

FIGURE 3.- CONCLUDED.

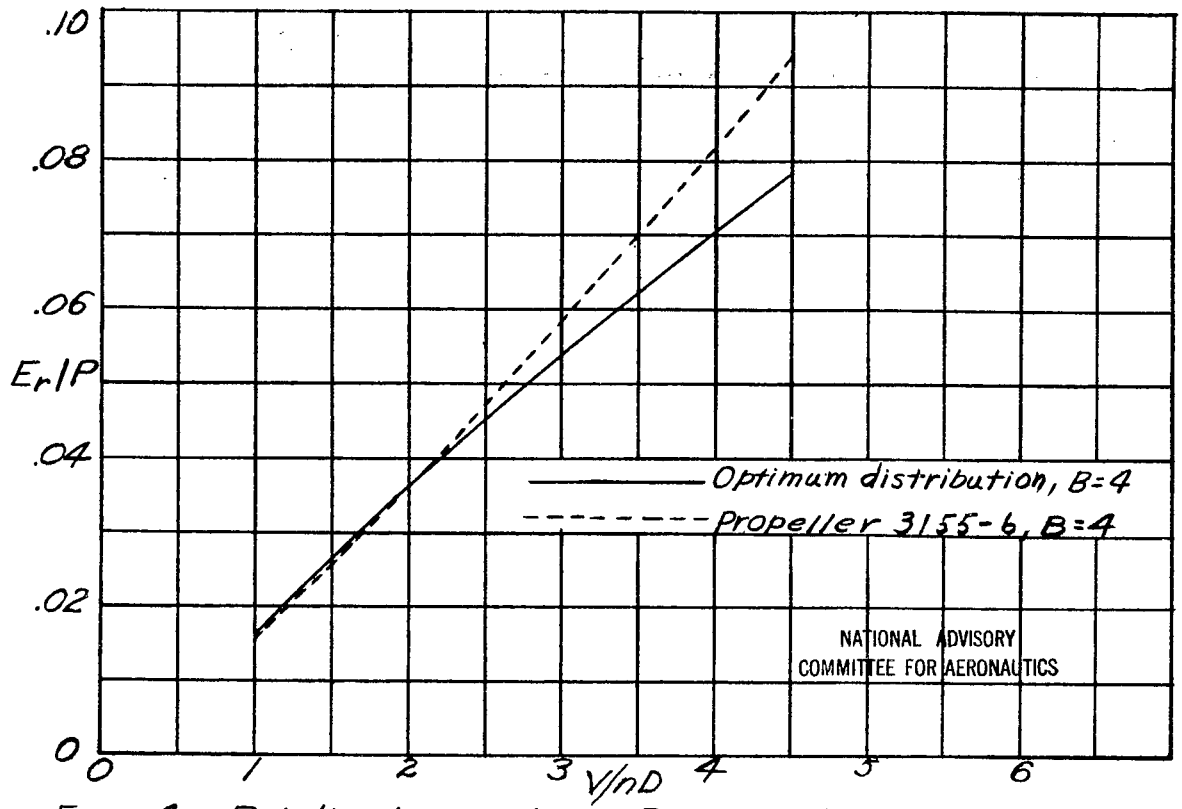

FIGURE 4.- Rotational-energy loss at R_2 corresponding to peak efficiency of four-blade Hamilton Standard 3155-6 propeller.

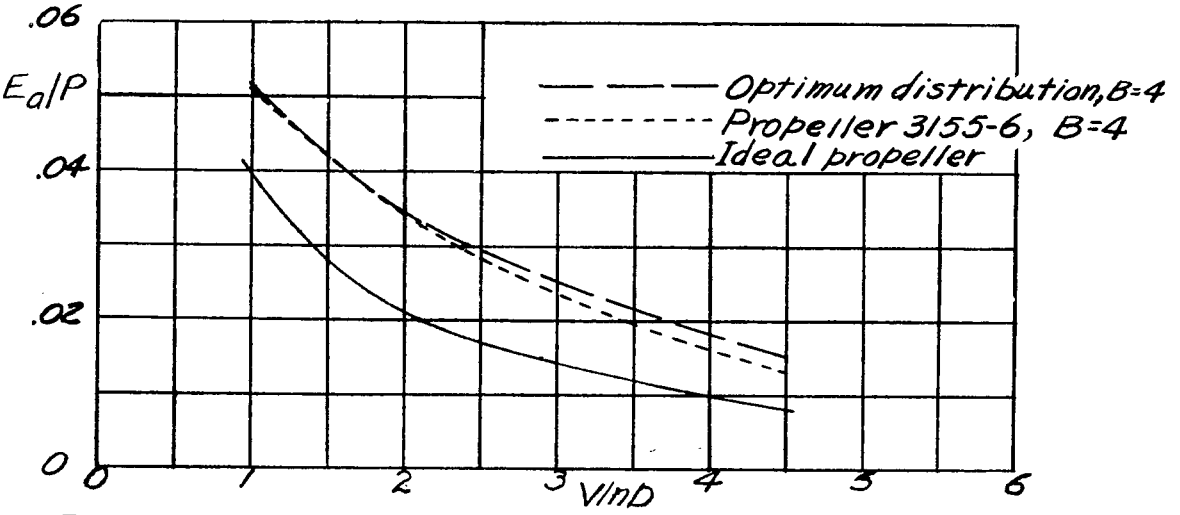

FIGURE 5.- Axial-energy loss at R_2 corresponding to peak efficiency of four-blade Hamilton Standard 3155-6 propeller.

[redacted]

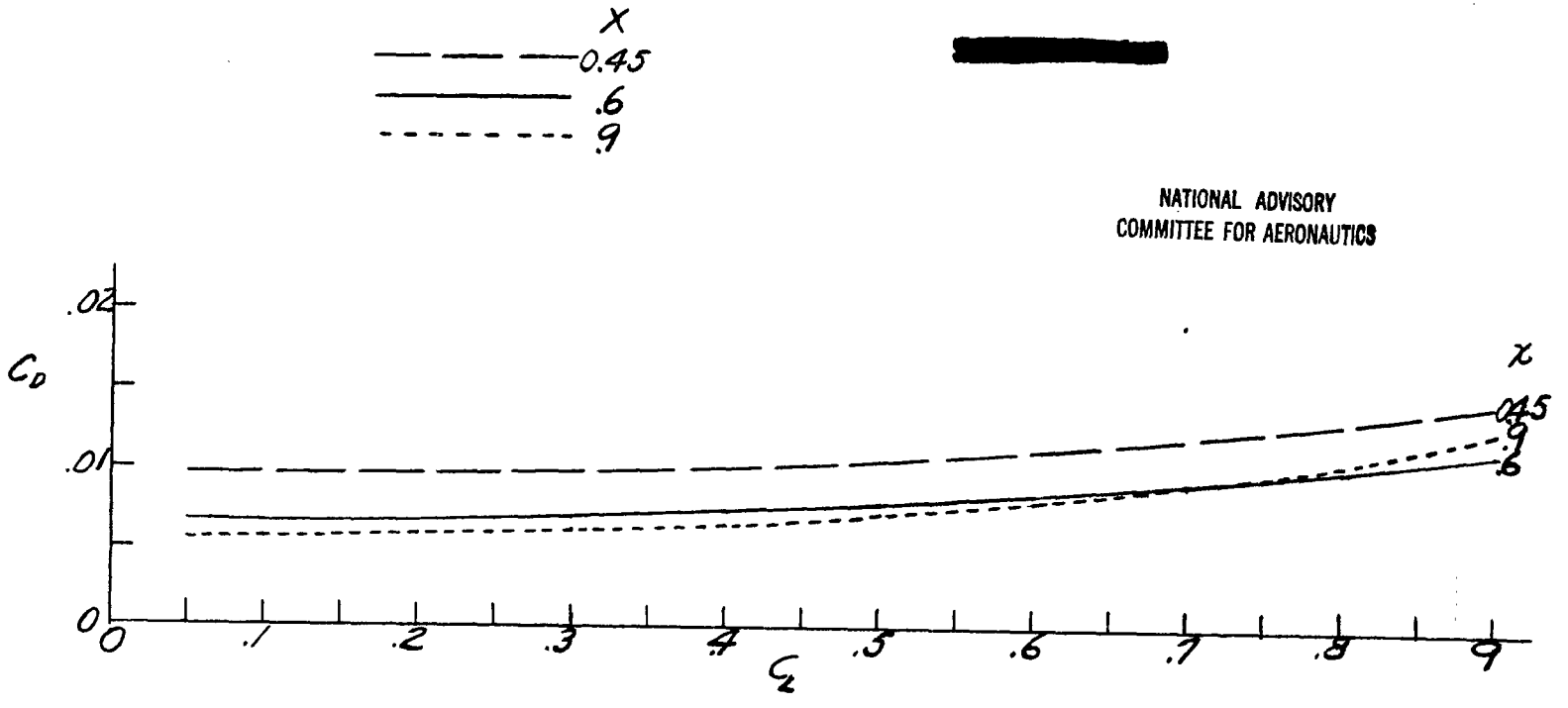

Figure 6.- Airfoil characteristics corrected to infinite aspect ratio for several blade sections. (Data from reference 7.)

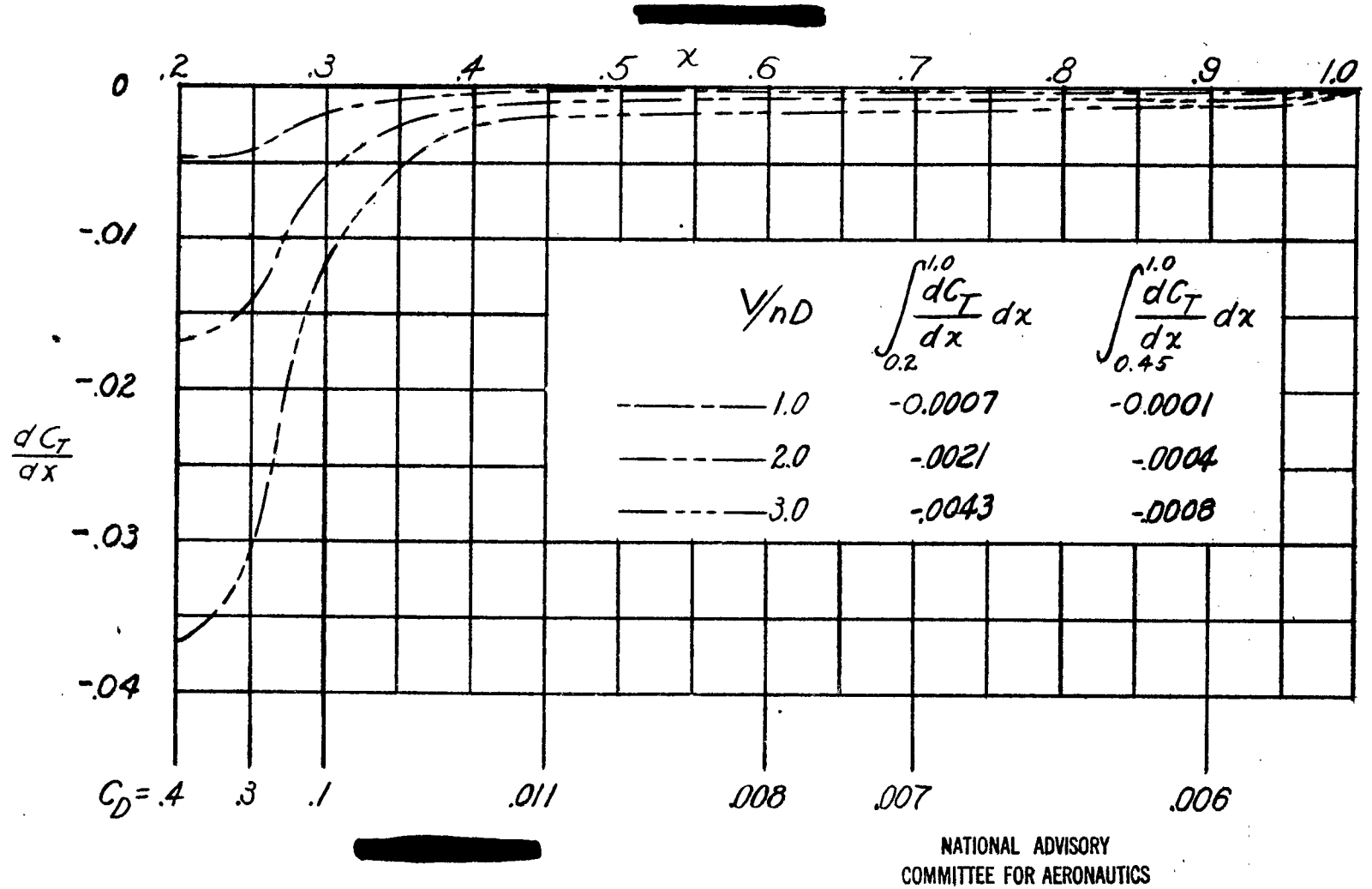

Figure 7.—Variation of thrust coefficient due to drag. B = 1.

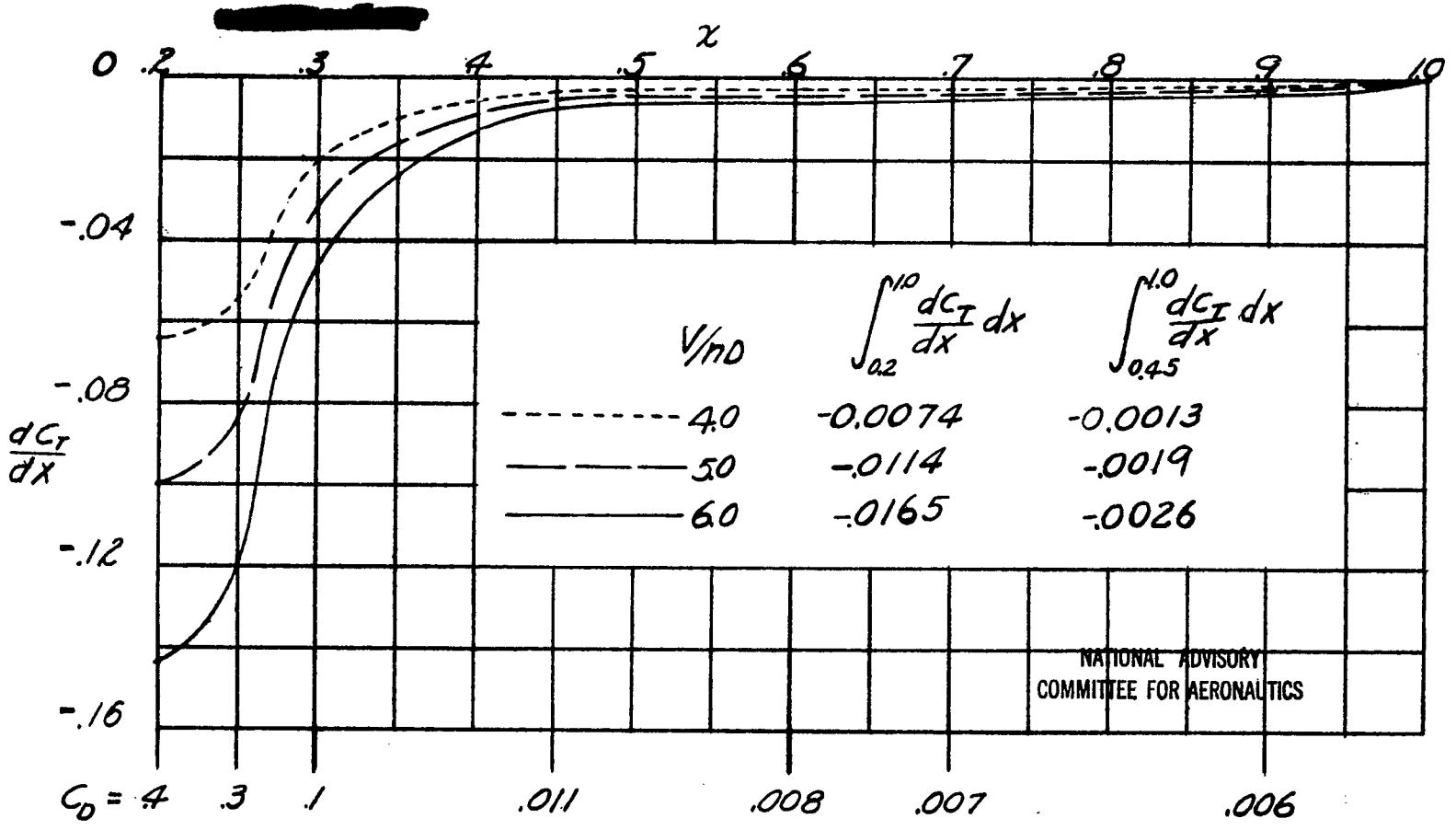

Figure 7. - Concluded.

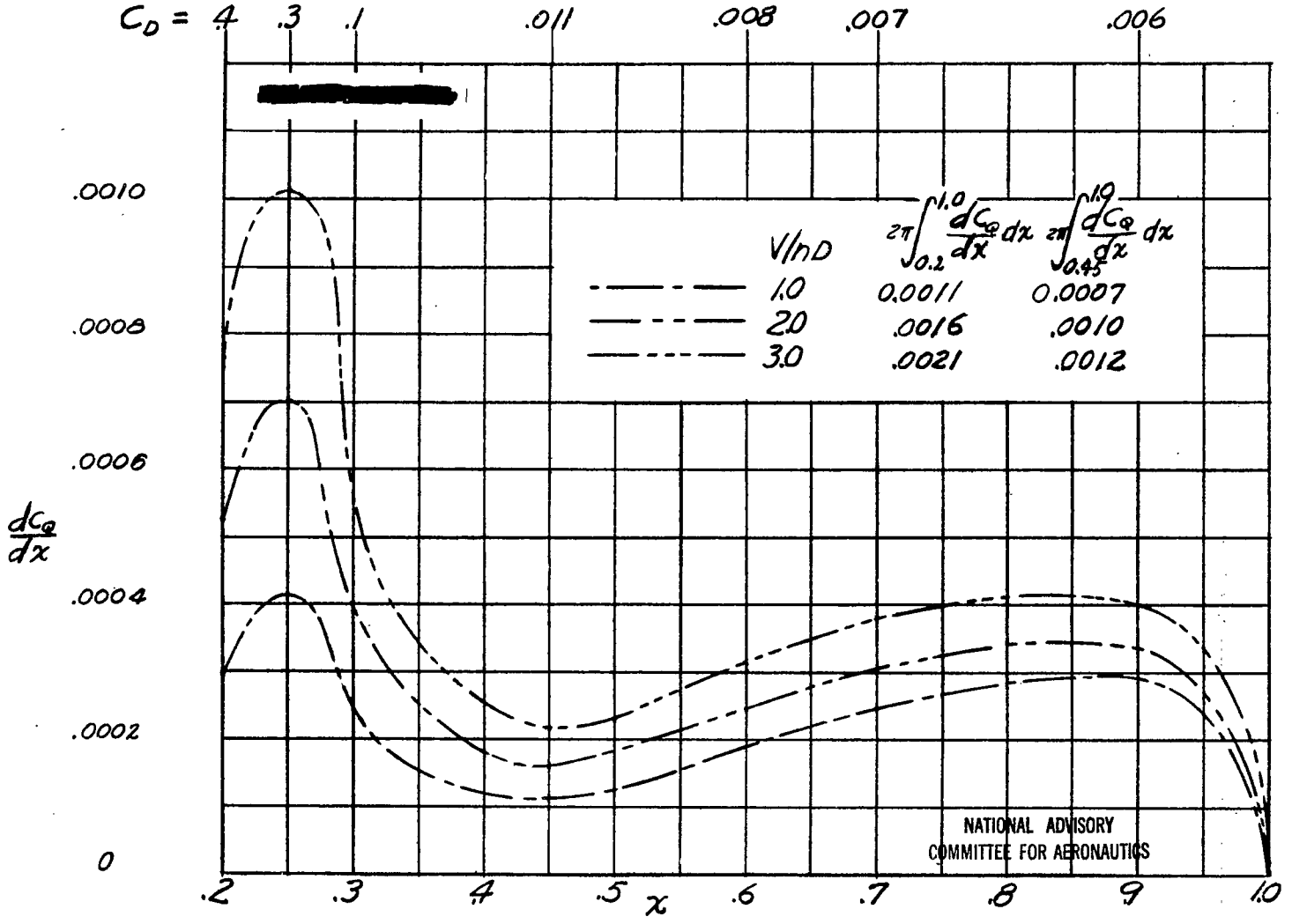

FIGURE 8.- VARIATION OF TORQUE COEFFICIENT DUE TO DRAG. B=1.

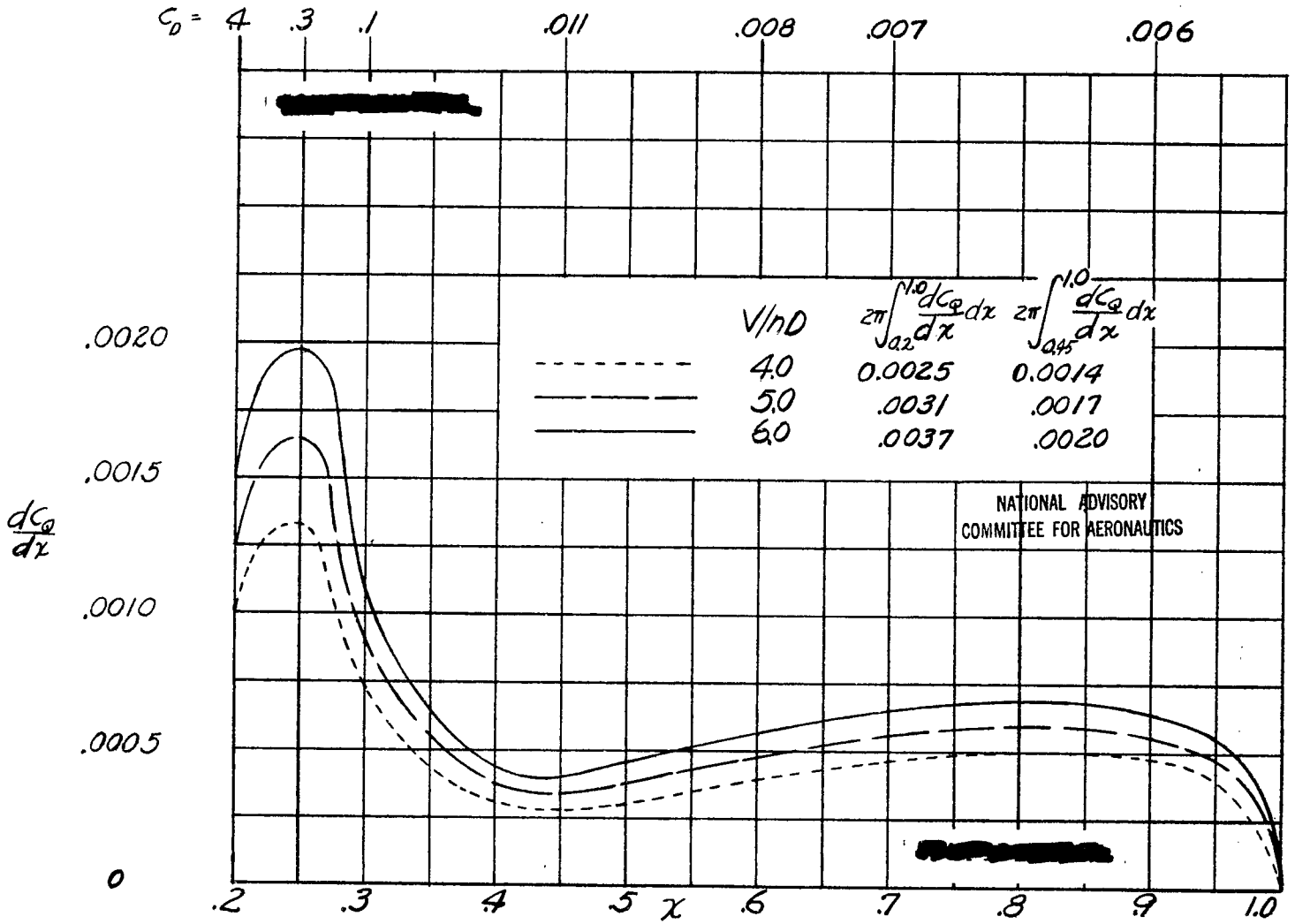

FIGURE 8.- CONCLUDED.

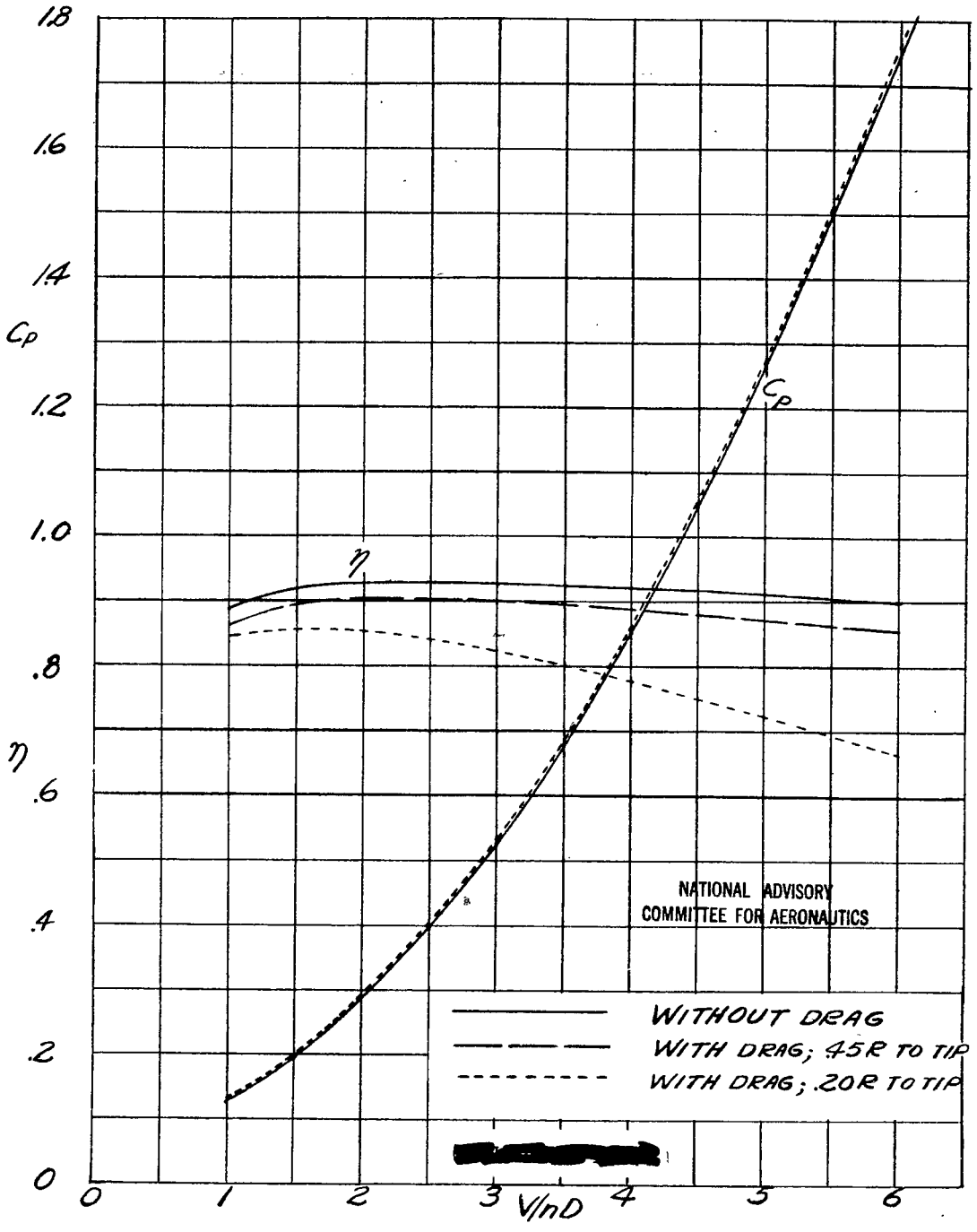

FIGURE 9.- EFFECT OF DRAG ON EFFICIENCY AND POWER COEFFICIENT AT PEAK EFFICIENCY FOR FOUR-BLADE HAMILTON STANDARD 3135-6 PROPELLER.

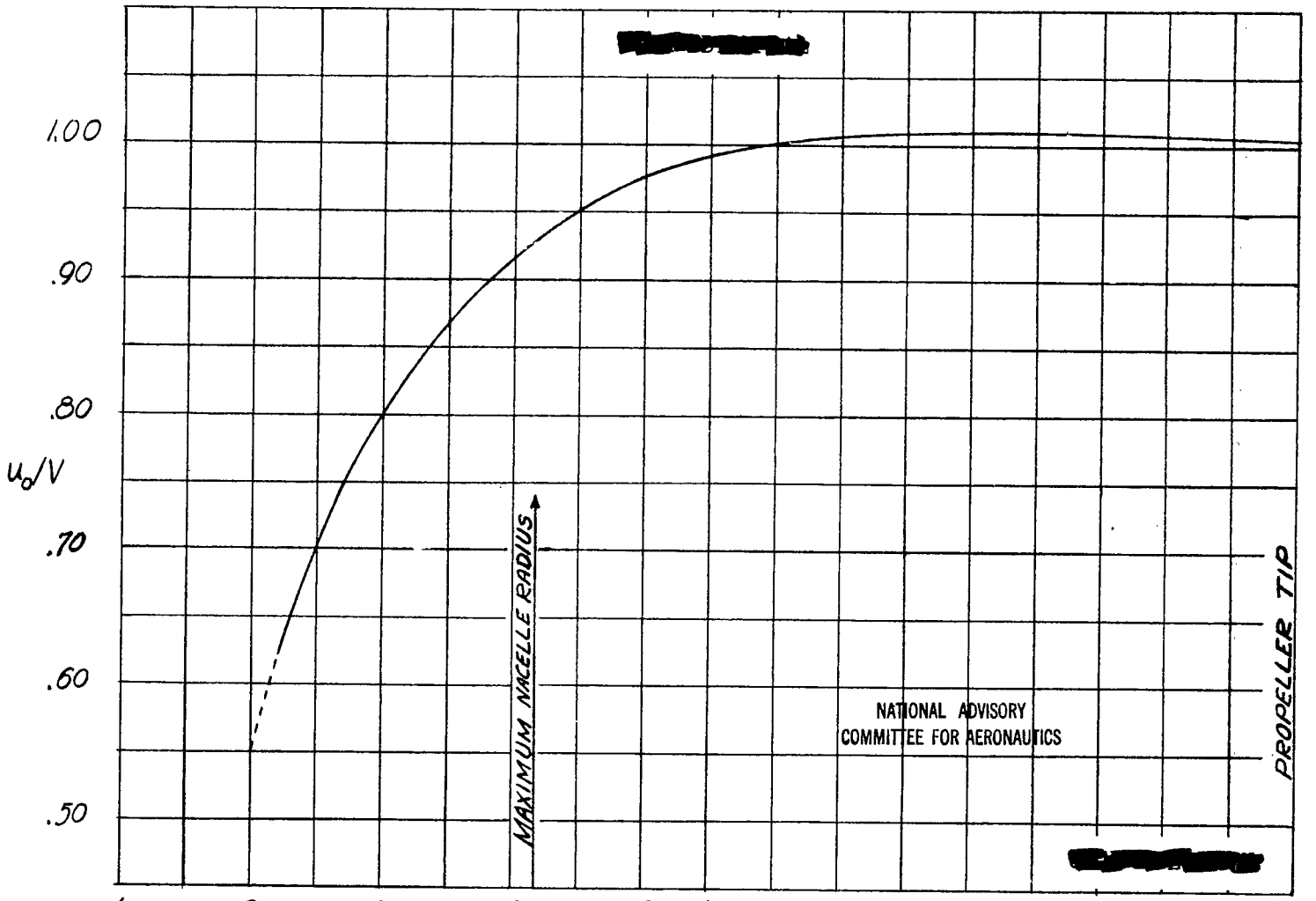

FIGURE 10.- VELOCITY DISTRIBUTION IN PLANE OF PROPELLER FOR NACA COWLING. PROPELLER REMOVED. (DATA TAKEN FROM REFERENCE 4.)

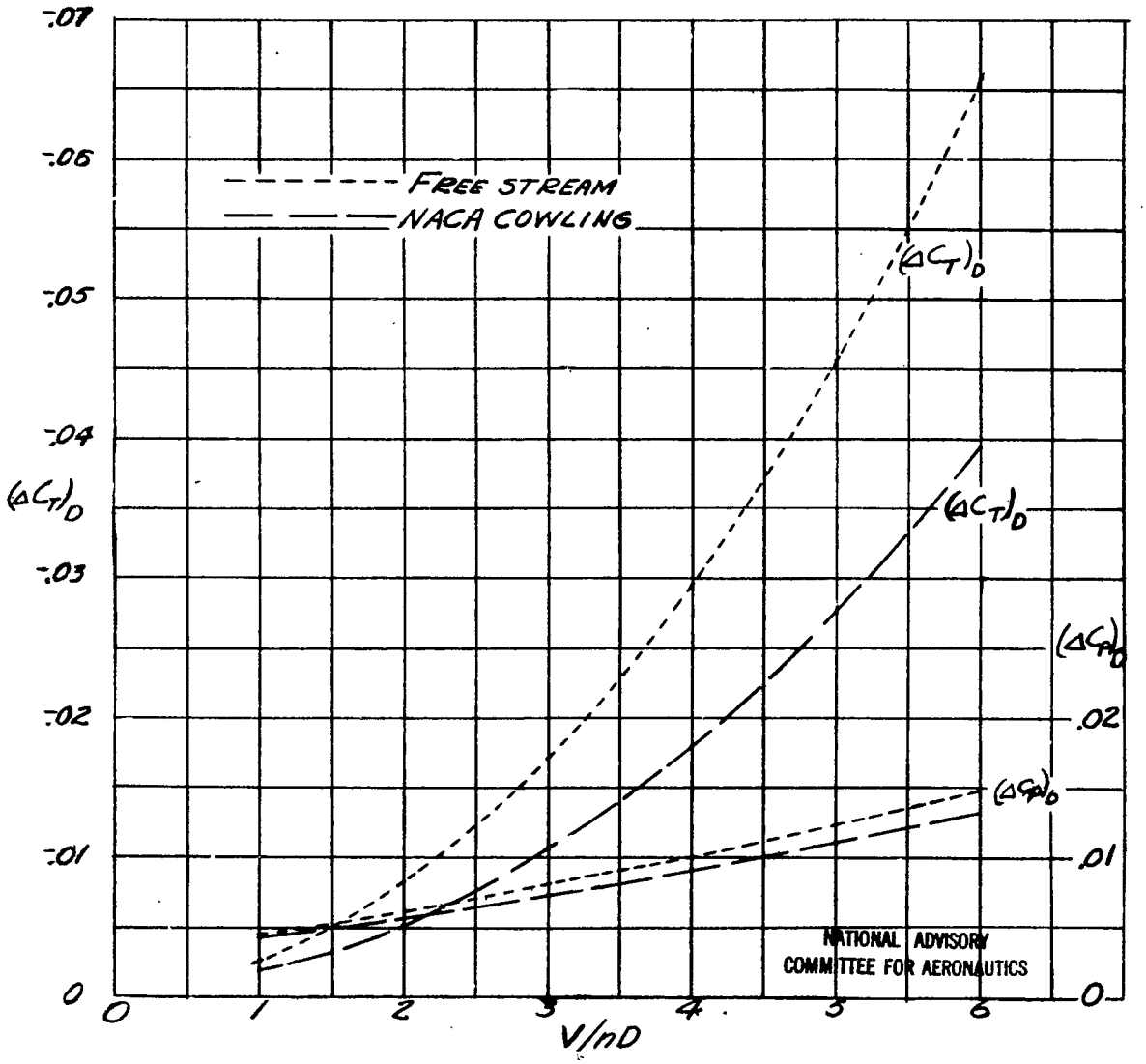

FIGURE 11.- VARIATION OF THRUST AND POWER COEFFICIENTS DUE TO DRAG WITH V/nD FOR CONSTANT DRAG DISTRIBUTION. B=4.

[redacted]

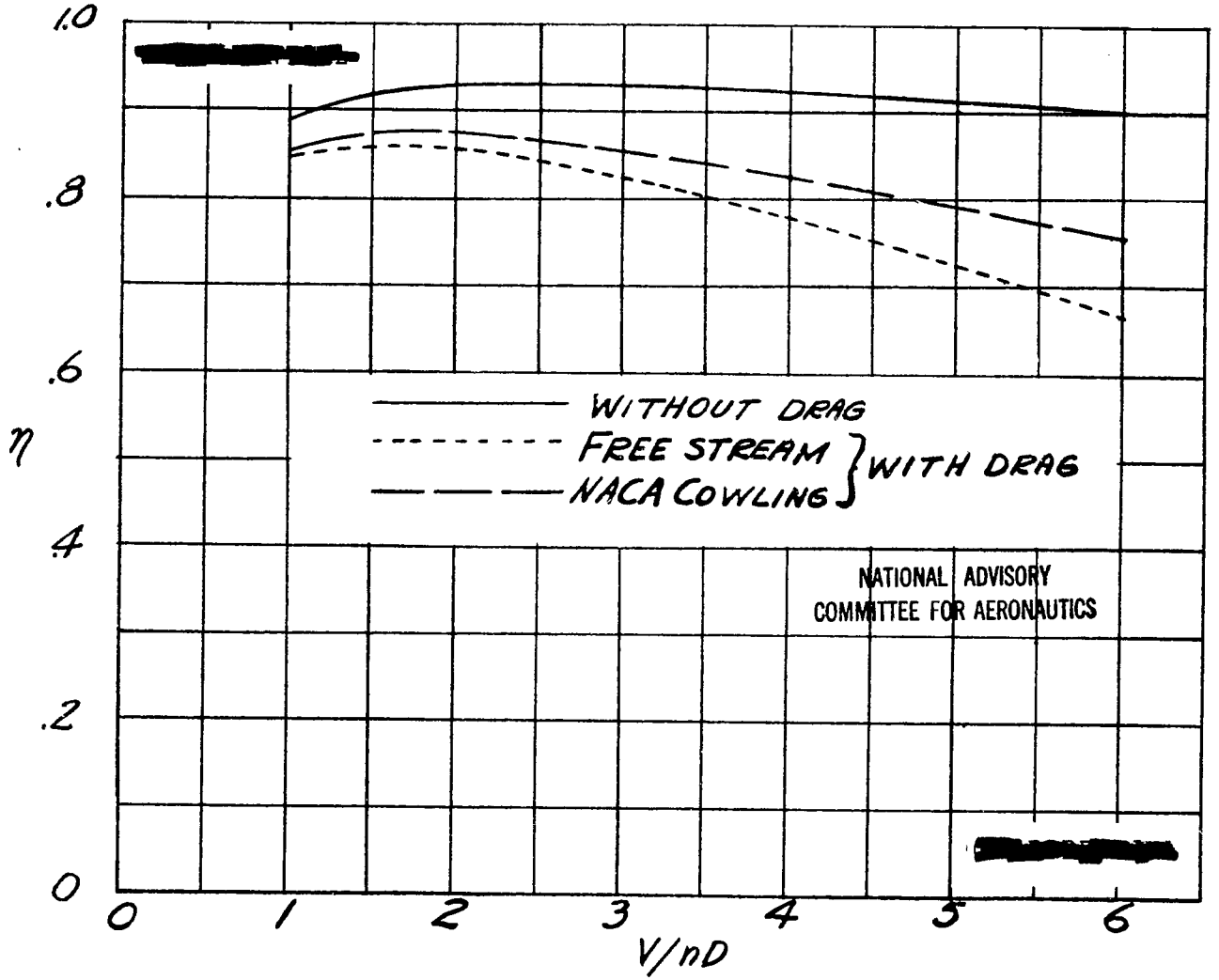

FIGURE 12— COMPARISON OF EFFICIENCIES OF FOUR-BLADE HAMILTON STANDARD 3155-6 PROPELLER.

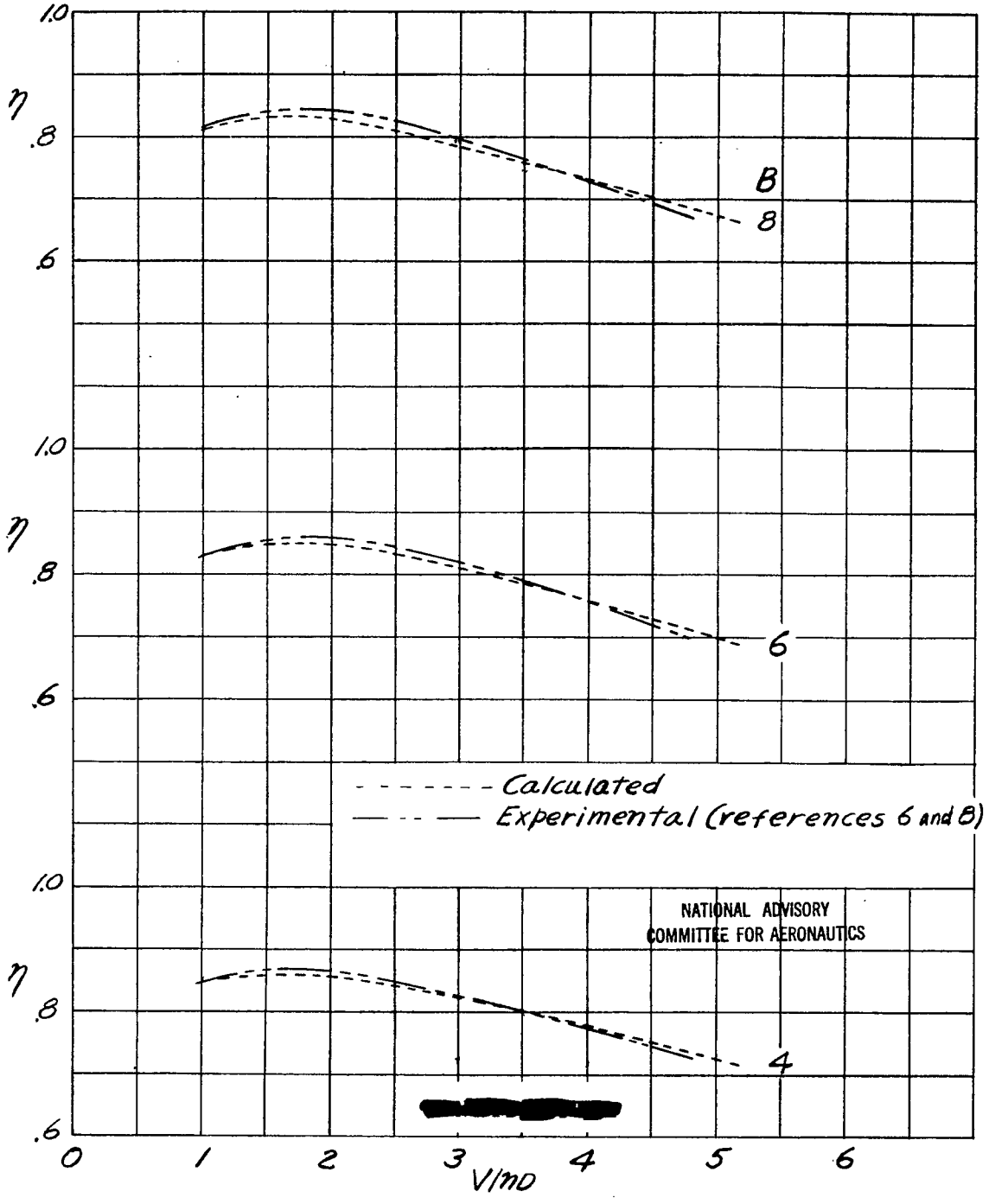

Figure 13.- Comparison of calculated and experimental propeller efficiency envelopes.

3 1176 00500 0816